



**POLITECNICO**  
**MILANO 1863**

**SCUOLA DI INGEGNERIA INDUSTRIALE  
E DELL'INFORMAZIONE**

## Space Systems Engineering and Operations

**Professor:** Michèle Roberta Lavagna

Academic year 2023-2024

## Solar and Heliospheric Observatory



Authors: Team 8		
Person Code	Surname	Name
10726940	Bachini	Pier Francesco A.
10721571	Belletti	Stefano
10764327	Bolsi	Pietro
10710062	De Magistris	Matteo
10737865	De Marco	Mattia
10713469	Topuz	Daniele

**Submission date:** Monday 9<sup>th</sup> September, 2024

# Contents

<b>List of Figures</b>	<b>iv</b>
<b>List of Tables</b>	<b>iv</b>
<b>1 SOHO mission overview</b>	<b>1</b>
1.1 Mission overview . . . . .	1
1.1.1 Mission drivers . . . . .	1
1.1.2 Functional analysis . . . . .	2
1.1.3 Mission phases . . . . .	2
Launch and Early Orbit Phase (LEOP) . . . . .	2
Transfer Trajectory Phase (TTP) . . . . .	2
Halo-Orbit Phase (HOP) . . . . .	3
1.1.4 ConOps . . . . .	3
1.2 Scientific payloads . . . . .	3
1.2.1 Payloads overview . . . . .	3
1.2.2 Mission scientific goals - Payloads correlation . . . . .	5
1.2.3 ConOps/Phases - Payloads correlation . . . . .	5
1.3 Mission analysis . . . . .	5
<b>2 Propulsion Subsystem</b>	<b>8</b>
2.1 Mission Analysis . . . . .	8
2.1.1 Preliminary mission trajectory design . . . . .	8
2.1.2 $\Delta v$ budget justification and retrieval . . . . .	9
2.2 Subsystem Description . . . . .	10
2.2.1 Architecture . . . . .	10
2.2.2 $\Delta v$ breakdown . . . . .	11
2.3 Structural sizing . . . . .	12
2.3.1 Propellant selection and margins . . . . .	12
2.3.2 Pressurant selection and sizing of the feeding system . . . . .	12
2.3.3 Tank sizing . . . . .	13
2.3.4 Mass budget . . . . .	14
2.3.5 Power budget . . . . .	14
2.3.6 Final configuration . . . . .	14
<b>3 TTMTTC subsystem</b>	<b>15</b>
3.1 Architecture . . . . .	15
3.1.1 TTMTTC components . . . . .	15
3.1.2 Modulation & encoding . . . . .	16
3.1.3 Transmission and Ground stations . . . . .	16
3.2 Mission phases correlation . . . . .	17
3.3 Sizing . . . . .	18
3.3.1 Losses . . . . .	18
3.3.2 Antennas . . . . .	18
3.3.3 Link budget equation . . . . .	19
3.3.4 Signal to noise ratio . . . . .	19
3.3.5 Results . . . . .	20

<b>4 AOCS subsystem</b>	<b>21</b>
4.1 Architecture . . . . .	21
4.1.1 Overview . . . . .	21
4.1.2 Sensors and Actuators . . . . .	21
Gyros: . . . . .	22
SSU: . . . . .	22
FPSS: . . . . .	22
SAS: . . . . .	22
RW: . . . . .	23
Thrusters: . . . . .	23
4.1.3 Redundancy . . . . .	23
4.2 Control Modes and Correlations . . . . .	23
4.2.1 Control Modes . . . . .	23
Normal Mode (NM): . . . . .	24
Emergency Sun Reacquisition (ESR) Mode: . . . . .	24
Initial Sun Acquisition (ISA) Mode: . . . . .	24
Roll Maneuver Wheels (RMW) Mode: . . . . .	25
4.2.2 Correlation with phases . . . . .	25
4.2.3 Pointing Budget . . . . .	25
4.3 Sizing . . . . .	25
4.3.1 Disturbances . . . . .	26
4.3.2 Modelling . . . . .	26
Reaction wheels . . . . .	26
Thrusters . . . . .	27
4.3.3 Results . . . . .	27
Power Budget . . . . .	27
Mass budget . . . . .	28
<b>5 TCS subsystem</b>	<b>29</b>
5.1 Architecture . . . . .	29
5.1.1 Overview . . . . .	29
5.1.2 Payload Module TCS . . . . .	29
5.1.3 Service Module TCS . . . . .	30
5.1.4 Interface Ring . . . . .	30
5.2 Mission phases correlations . . . . .	31
LEOP . . . . .	31
TTP . . . . .	31
HOP . . . . .	31
5.3 Sizing . . . . .	31
5.3.1 Spacecraft modelling . . . . .	31
5.3.2 Modelling . . . . .	32
5.3.3 Results . . . . .	33
Hot case - TTP . . . . .	33
Cold case - L1 . . . . .	33
Coupled case . . . . .	34
5.3.4 Budget . . . . .	34
5.3.5 Conclusions . . . . .	34

<b>6 EPS subsystem</b>	<b>35</b>
6.1 Architecture . . . . .	35
6.1.1 Overview . . . . .	35
6.1.2 Power Management . . . . .	35
Power Control . . . . .	35
Solar Arrays . . . . .	35
Batteries . . . . .	35
6.1.3 Main parameters . . . . .	36
6.2 Mission phases correlations . . . . .	36
6.2.1 Power demands . . . . .	36
6.2.2 Phases . . . . .	37
LEOP . . . . .	37
TTP . . . . .	37
HOP . . . . .	37
6.2.3 Modes . . . . .	37
6.2.4 Considerations . . . . .	38
6.3 Sizing . . . . .	38
6.3.1 Solar Arrays . . . . .	38
6.3.2 Batteries . . . . .	40
<b>7 Space Segment &amp; OBDH</b>	<b>41</b>
7.1 Space Segment . . . . .	41
7.1.1 Configuration . . . . .	41
Payload module . . . . .	41
Propulsion subsystem . . . . .	42
TTMTC subsystem . . . . .	42
ADCS subsystem . . . . .	42
Thermal subsystem . . . . .	43
Power subsystem . . . . .	43
7.1.2 CAD representation . . . . .	43
7.2 OBDH . . . . .	44
7.2.1 Architecture . . . . .	44
Overview . . . . .	44
Management . . . . .	44
Bus . . . . .	44
Memory . . . . .	44
Computational units . . . . .	45
Time . . . . .	45
Data protocol . . . . .	45
7.2.2 OBDH Sizing . . . . .	45
<b>8 References</b>	<b>48</b>

## List of Figures

1	SOHO S/C <sup>[1]</sup> . . . . .	1
2	Functional analysis . . . . .	2
3	SOHO ConOps . . . . .	3
4	SOHO trajectory . . . . .	6
5	Computed trajectory . . . . .	9
6	SOHO - blow-down architecture . . . . .	10
7	SOHO - propulsion module <sup>[2]</sup> . . . . .	10
8	SOHO - TTMTTC architecture . . . . .	15
9	Normal Mode routine operations - 24 hours <sup>[3]</sup> . . . . .	18
10	SOHO visibility - 24 hours . . . . .	18
11	SOHO - AOCS architecture . . . . .	23
12	TCS Subdivision <sup>[4]</sup> . . . . .	29
13	SOHO Sunshield Enclosure <sup>[4]</sup> . . . . .	30
14	EPS Architecture with telemetry parameters (see Table 26) . . . . .	35
15	SOHO launch configuration <sup>[5]</sup> . . . . .	41
16	CAD <sup>[6,7]</sup> of the SOHO S/C . . . . .	43
17	OBDH architecture <sup>[8]</sup> . Duplicated rectangles indicate duplicated hardware . . . . .	44

## List of Tables

1	Scientific goals - Payloads correlation . . . . .	5
2	Correlation between ConOps/phases and on-board instruments . . . . .	5
3	Launcher components information . . . . .	6
4	Budget expectations <sup>[9]</sup> . . . . .	8
5	True $\Delta v$ . . . . .	8
6	Computed $\Delta v$ . . . . .	9
7	Total True/Computed $\Delta v$ . . . . .	9
8	Desired $\Delta v$ Direction - Used DTM - Parasitic Torque Axis <sup>[10]</sup> . . . . .	11
9	Manoeuvres until trim <sup>[11]</sup> . . . . .	11
10	Station keeping manoeuvres <sup>[12]</sup> . . . . .	11
11	Comparison between sizing and real data . . . . .	14
12	Instruments data rates <sup>[13,14]</sup> . . . . .	16
13	Antenna gains for uplink and downlink . . . . .	18
14	Parameters . . . . .	20
15	Results . . . . .	20
16	Sensors . . . . .	22
17	Actuators . . . . .	22
18	Maximum power consumption . . . . .	28
19	Mass budget . . . . .	28
20	SOHO thermal data <sup>[4]</sup> . . . . .	32
21	Instruments temperatures <sup>[4,15]</sup> . . . . .	32
22	Exchanged power hot case, TTP . . . . .	33
23	Exchanged power cold case, L1 . . . . .	33
24	Coupled case results . . . . .	34
25	Thermal control budget . . . . .	34
26	Telemetry parameters <sup>[16]</sup> . . . . .	36
27	Payloads power requirements <sup>[17]</sup> . . . . .	36
28	Subsystems power requirements <sup>[4,18,19]</sup> . . . . .	37

29	Payloads information <sup>[17]</sup>	41
30	Payloads enumeration <sup>[20,21]</sup>	43
31	dedicated memory <sup>[14]</sup>	45
32	Data handling specifications <sup>[14]</sup>	45
33	OBDH worst case scenario: station keeping	47
34	Station keeping	47
35	Nominal mode	47

# 1 SOHO mission overview

## 1.1 Mission overview



Figure 1: SOHO S/C<sup>[1]</sup>

The Solar and Heliospheric Observatory (SOHO) is a space mission that forms part of the *Solar-Terrestrial Science Program* (STSP), developed in a collaborative effort by the European Space Agency (ESA) and the *National Aeronautics and Space Administration* (NASA). The STSP constitutes the first “cornerstone” of ESA’s long-term program known as *Space Science Horizon 2000*.

SOHO was launched by an Atlas II-AS on the 02/12/1995 and is currently placed in a halo orbit around the Sun-Earth L1 Lagrangian point where it is pointing to the Sun centre with an accuracy of 10 arcsec. Telemetry is received by NASA’s *Deep Space Network* (DSN), while planning, coordination and operation of the spacecraft and the scientific payload are conducted from the *Experiment Operations Facility* (EOF) at NASA’s *Godard Space Flight Center* (GSFC).

The mission was meant to last 2 years, until 1998, but given its success it was prolonged by ESA and NASA with several mission extensions: the mission is still ongoing.

SOHO is a three-axis stabilized spacecraft measuring approximately 4.3 x 2.7 x 3.65 meters (9.5 meters with solar arrays deployed) and a total mass of 1850 kg; it can generate power up to 1500 W. The payload weighs about 610 kg and consumes 450 W during operations.

The principal scientific objectives of the mission are:

- Study the solar interior, using techniques of helioseismology
- Study the heating mechanisms of the solar corona
- Investigate the solar wind and its acceleration processes

To achieve these goals, SOHO carries a payload consisting of 12 sets of complementary instruments that allow to study phenomena initiated by processes commencing below the photosphere and propagating up the corona. It also carries a complement of instruments whose aim is to study the oscillations on the solar surface by measuring the velocity (via Doppler effect) and its intensity changes produced by pressure and gravity waves.

### 1.1.1 Mission drivers

Mission Drivers are set to better specify the presence of highly sensitive mission elements that are particularly delicate for the mission outcome. These can be summarized as:

#### 1. Completing the halo insertion trajectory & operate around the first Sun-Earth Lagrangian point

The S/C shall perform all the needed manoeuvres and corrections in order to be able to reach the designated working location and remain in this area.

#### 2. Being able to work in the harsh conditions of space

The S/C shall be able to survive in a region with high concentration of ionized particles and radiations and constantly exposed to solar winds.

### 3. Being able to transfer data with the ground stations (GS)

The S/C shall be able to communicate with a control center in order to exchange communications and scientific data; for this reason it also shall be able to produce electric power, using the solar arrays.

#### 1.1.2 Functional analysis

In order to achieve its objectives, the spacecraft must perform a set of functions, described through the functional analysis<sup>[8,14,22]</sup> as can be seen in Figure 2:

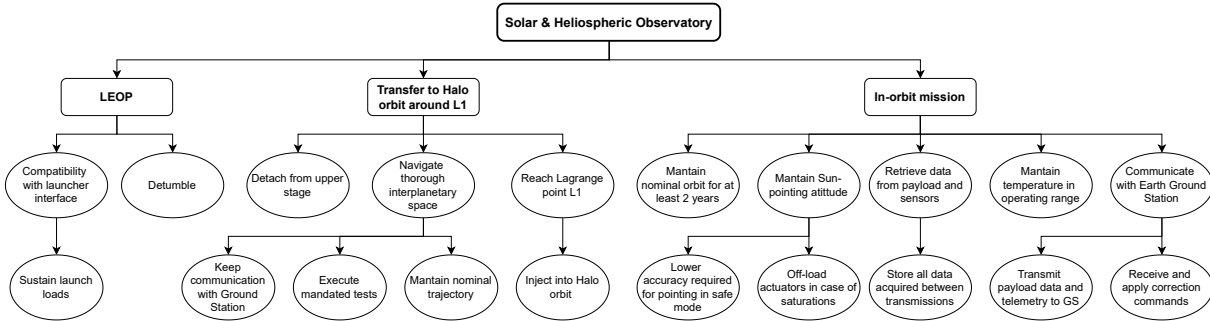


Figure 2: Functional analysis

#### 1.1.3 Mission phases

**Launch and Early Orbit Phase (LEOP)** This first phase starts at lift-off and ends when the spacecraft is injected into the transfer orbit towards the L1 Lagrangian point. It is divided in two main sub-phases:

**Ascent Sub-phase (2 - 4 December 1995):** Lift-off until the injection into the near-circular parking orbit. SOHO was launched by an Atlas II-AS with a Centaur upper stage, which gave the first burn to inject into the parking orbit. Right after the ascent, deployment of the solar arrays was performed.

**Parking Orbit Sub-phase (4 December 1995 - 4 January 1996):** Injection into parking orbit until the injection into transfer orbit. The Centaur upper stage initially achieved a 185 km x 175 km parking orbit; then, following an 80 min coast period, a second burn injected SOHO into a transfer trajectory towards the L1 point.

**Transfer Trajectory Phase (TTP)** The TTP starts with the injection into the transfer orbit and ends with the injection into the L1 halo orbit. It is divided in the following sub-phases:

**PRE-SEP Sub-phase (35 minutes):** Injection into transfer orbit until the separation from the Centaur upper stage.

**PRE-OP Sub-phase (3 hours):** Await for separation until the anti-Sun line/spacecraft/Earth angle is less than 33 degrees.

**Low Rate Sub-phase (4 hours):** Beginning of Sun pointing, low-gain antennas available for low data rate transfer only.

**High Rate Sub-phase (4 January 1996 - 14 February):** High-gain antennas deployed for the remainder of the TTP.

**Halo-Orbit Phase (HOP)** The HOP begins at the halo orbit injection, and is composed of:

**Commissioning Sub-phase (1 month):** Injection into halo orbit and await for check-out and commissioning of all the on-board instruments.

**Mission Operations Sub-phase:** Started after commissioning, it includes all scientific and routine operations necessary for the experiment activities. Orbit maintenance manoeuvres should be conducted after insertion and then every 8 weeks. During this phase, the satellite is three-axis-stabilised in a Sun-pointing attitude. In case of safe-mode activation, the S/C maintains the Sun-pointing attitude but with a lower accuracy.

Three daily passes of 1.6 h and one 8 h pass are baselined for support during 10 months per year, the remaining 2 months having 24 h/day support. The on-board data recorder provides data storage during all non-contact periods.

SOHO was declared fully commissioned on 16 April 1996.

### 1.1.4 ConOps

The ConOps of the mission are presented in Figure 3, from launch to the predicted end of life of the mission<sup>[8,22,23]</sup>:

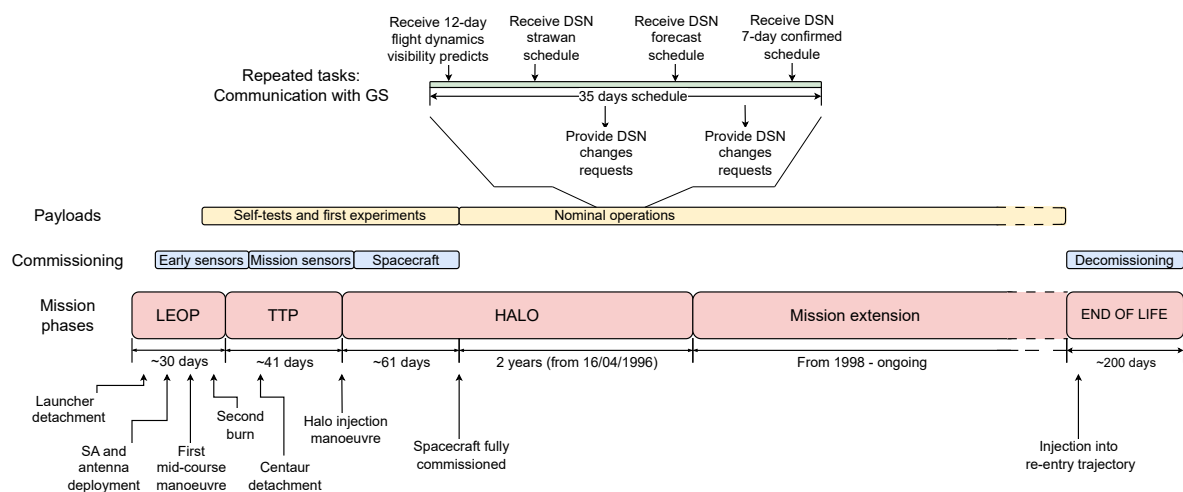


Figure 3: SOHO ConOps

## 1.2 Scientific payloads

### 1.2.1 Payloads overview

SOHO is equipped with 12 different scientific instruments. They can be divided into three main categories based on the scientific goals of the mission: helioseismology, coronal and solar wind “in-situ” study instruments<sup>[13,24]</sup>.

**GOLF (Global Oscillations at Low Frequencies):** it measures the low degree global solar velocity oscillations ( $\ell \leq 3$ ) using a very stable sodium-vapour resonance scattering spectrometre with a sensitivity better than 1 mm/s over the complete frequency range from 0.1  $\mu$ Hz to 6 mHz (periods from 3 min to 100 days). Furthermore, it measures the long-term variations of the global average of the line-of-sight magnetic field (precision of 1 mG).

**VIRGO (Variability of solar IRradiance and Gravity Oscillations):** it measures the low degree ( $\ell \leq 7$ ) solar intensity oscillations with relative accuracy better than 1 ppm; it also provides measurements of the solar constants with absolute accuracy better than 0.15%.

**SOI (Solar Oscillations Investigations):** using the Michelson Solar Imager (MDI) it measures the solar velocity oscillations in the harmonic degree ( $\ell$  up to 1500) and high degree ( $\ell$  up to 4500). It can execute four different observing programs (“structure”, “dynamics”, “campaign” and “magnetic field” program).

**SUMER (Solar Ultraviolet Measurements of Emitted Radiation):** it is a UV telescope equipped with a normal incidence spectrometer (UV lines in the range 500 to 1600 Å), capable of studying the plasma flows characteristics (temperature, density, wave motions) in the upper chromosphere, transition region and corona; it should also be capable of measuring the velocity fields in the transition region and corona with a resolution of 1 km/s.

**CDS (Coronal Diagnostic Spectrometer):** it's a telescope equipped with two spectrometers; it provides measurements of both absolute and relative intensities of selected EUV lines (wavelenght from 150 to 800 Å) to determine temperatures and densities of coronal structures.

**EIT (Extreme-ultraviolet Imaging Telescope):** it provides full Sun high resolution EUV images in four emission lines corresponding to four different temperatures, completing the measurements taken by SUMER and CDS.

**UVCS (UltraViolet Coronagraph Spectrometer):** it's a telescope equipped with high resolution spectrometers which make observations of the solar corona (1.3 - 10 R<sub>☉</sub>) to study the origin and acceleration of the solar wind, and the heating of coronal plasma too.

**LASCO (Large Angle and Spectrometric CORonagraph):** it consists of three coronagraphs with different fields of view (1.1 - 30 R<sub>☉</sub>) which study the evolution of the solar corona and the mass, momentum and energy transport in it.

**SWAN (Solar Wind ANisotropies):** it consists of two periscopes capable of mapping a full hemisphere with a 1 deg resolution; it measures the latitude distribution of the solar wind mass flux from the equator to the pole by mapping the emissivity of the Ly- $\alpha$  light.

**CELIAS (Charge, EElement and Isotope Analysis System):** it consists of three mass-and-charge-discriminating sensors and measures the mass, ionic charge and energy of the low and high speed solar wind, of suprathermal ions and of low energy flare particles. Furthermore, it includes the photodiode spectrometer SEM (Solar Extreme-ultraviolet Monitor) which makes measurements of the solar flux.

**COSTEP (COnprehensive SupraThermal and Energetic Particle analyser):** by using solid state and plastic scintillator detectors, it measures the energy spectra of electrons (up to 5 MeV), protons and He nuclei (up to 53 MeV/nuc). Its measurements will support studies on the energy release and particle acceleration processes in the solar atmosphere and particle propagation in the interplanetary medium.

**ERNE (Energetic and Relativistic Nuclei and Electron experiment):** it uses the same principles of COSTEP and measures the energy spectra of elements in the range Z=1-30 (up to 50 MeV/nuc), abundance ratios of isotopes and anisotropies of the particle flux.

### 1.2.2 Mission scientific goals - Payloads correlation

Scientific Goals	Payloads & Measurements
Helioseismology experiments to measure solar pressure ( $p$ ) and gravity ( $g$ ) oscillation modes.	GOLF and VIRGO for the low frequency modes, SOI/MDI for the harmonic and high frequency modes.
Investigation of the dynamics and evolution of the physical structure of the solar corona.	CDS (temperature and density), SUMER (velocity and turbulence), EIT (imaging at different temperatures) in the corona; LASCO (electron density), UVCS (temperature and velocity) in the outer corona; SWAN (density) in the outermost corona and solar wind.
Investigation “in-situ” of the composition of the solar wind and energetic particles, from its generation to its acceleration process.	CELIAS (energy distribution and composition), COSTEP (energy distribution of ions and electrons), ERNE (energy distribution and isotopic composition of ions and electrons).

Table 1: Scientific goals - Payloads correlation

### 1.2.3 ConOps/Phases - Payloads correlation

Phases/ConOps	Payloads
LEOP	Early commissioning of the payloads and subsystems.
TPP	Initial experiments conducted to continue the commissioning of the payloads and the evaluation of the subsystems using data acquired by the payloads (e.g. thermal evaluation with solar constant's values measured by VIRGO; absolute pointing evaluation with data from CDS, EIT, LASCO, MDI, SUMER, UVCS and VIRGO).
HOP	Remaining commissioning experiments; beginning of the nominal operations with data acquisition from the payloads, data storage and transmission to Ground Segment.

Table 2: Correlation between ConOps/phases and on-board instruments

## 1.3 Mission analysis

Since the purpose of the mission is to monitor the Sun activity without interference from Earth and its atmosphere interaction, the observation takes place at the Lagrange point L1, which is unstable on a time scale of approximately 23 days but provides a smooth Sun-S/C velocity change throughout the orbit, that is required to obtain accurate helioseismology measurements: the period around the L1 point (in the final orbit) is about 178 days. The characteristic semi-diameters of this orbit are approximately 200'000 km in the ecliptic in Earth-Sun direction and 650'000 km in the ecliptic perpendicularly to Earth-Sun direction. The Lagrange point is at a distance of about 1.5 million km from Earth in Sun direction, aligned with the two bodies. Its position slightly changes during the year due to Earth's orbit not being exactly circular.

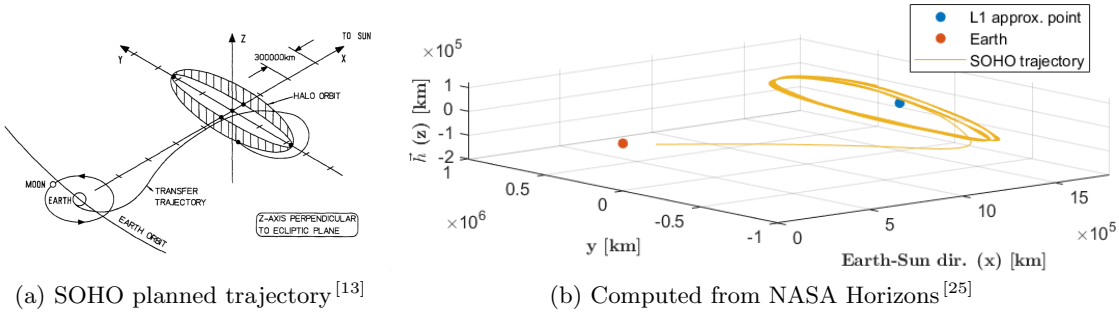


Figure 4: SOHO trajectory

The launch is scheduled on a two stages Atlas II-AS AC-121, and the S/C is equipped with fuel sufficient for a mission duration of 6 years.

At lift-off, the vehicle is approximately 47.4 m tall, 4 m in diameter and weights 236'268 kg. The Atlas consists of a solid rocket booster stage powered by four Thiokol Castor IV-A solid rocket boosters and a core vehicle stage (booster with two chambers and a sustainer) powered by Rocketdyne MA-5A liquid propellant engines (RP-1 fuel and liquid oxygen)<sup>[26,27]</sup>.

The multiple firing Centaur is powered by two Pratt & Whitney (RL10A-4) liquid hydrogen and liquid oxygen engines with extensible nozzles. Vehicle guidance and range safety is mounted on the Centaur stage. The Centaur rocket body is 3.04 m in diameter, 9 m tall and weights 1814 kg empty.

SOHO maneuvering capability is provided by a blow-down monopropellant hydrazine propulsion system. The fuel, 251 kg at launch, is carried by a single tank of prolate spheroidal shape. The total  $\Delta V$  capability at launch was approximately 318 m/s (neglecting canting and plume impingement losses), though only 275 m/s of that was allocated to the overall  $\Delta V$  budget. The leftover was reserved for attitude control, including momentum management maneuvers<sup>[28]</sup>.

Given the information about the launcher masses<sup>[26,29]</sup>:

	Thiokol Castor IV-A	Atlas MA-5AS	Atlas II-AS	Centaur II-A	SOHO S/C
Stage	0	1	1	2	Payload
Motors	4	1	1	1	-

	$m_G$ [kg]	$m_E$ [kg]	$t_B$ [s]	$I_{sp}$ [s]	$I_{sp_{sl}}$ [s]	T [kN]	$T_{sl}$ [kN]
Thiokol Castor IV-A	11567	1455.7	55.2	-	237.8	-	433.7
Atlas MA-5AS	-	-	283	293.4	262.1	2.065	1.854
Atlas II-AS	-	-	283	311	216.1	380.6	266
Atlas B+S	166748	10348	283	310.9	216.4	382.7	267.9
Interstage Adapter	545	545	-	-	-	-	-
Fairing	2087	2087	-	-	-	-	-
Centaur II-A	18770	1840	377.12	450.5	-	198.4	-
SOHO S/C	1850	1599	-	220	-	0.0042	-

Table 3: Launcher components information

Using the Tsiolkovsky Rocket formula:

$$\Delta V_{stage} = I_{sp} g_0 \ln \left( \frac{m_i}{m_f} \right) \quad (1)$$

We derived the theoretical maximum  $\Delta V$  budget for the whole mission, as summation of the  $\Delta V_i$  of each stage, based on the Launcher and S/C characteristics:

$$\Delta V_{budget} = \sum_{i=1}^{N_{stages}} \Delta V_{stage,i} = 13.391 \text{ km/s} \quad (2)$$

The “Stage 0”, composed of the four Thiokol solid boosters, has two different ignitions: the first starts with the starting of the Atlas motors, and take two Thiokol Castor, that separate from the rocket body as soon as the burning time (referred as  $t_B$  in Table 3) of  $55.2\text{s}$  finishes. The second ignition involves the last pair of Thiokol Castor and starts immediately after the detachment of the first pair. The remaining burning time for the “Stage 1” is of  $283\text{s} - 2*55.2\text{s} = 172.6\text{s}$ , then it also detaches from the rocket body, together with the Inter-stage Adapter and the Fairing.

The group computed the estimated cost for the mission taking into account every milestone and by considering the following assumptions, given the peculiar trajectory of the S/C: for the departure, it was considered the parabolic escape velocity from the Earth (since L1 is outside of the Sphere Of Influence of the planet), while for the other manoeuvres the group relied on the telemetry available from NASA Horizons<sup>[25]</sup>. Variations of velocity in time have been analyzed, using plotted graphs of the obtained delta velocity of the mission, and by identifying the peaks (those corresponding to motors ignition) and then evaluating the difference in speed (considered as impulsive, given the relatively small time of burn), making sure of not considering the variation due to normal gravity influence. The position of the velocity peaks is coherent with the mission schedule found<sup>[30]</sup>.

The milestones of the mission can be summarized as:

- **Launch:** The mission starts on December 2, 1995 at 08:08:01 UT/GMT from Cape Canaveral Air Station (Florida, USA). Initially, the S/C is injected into a low Earth parking orbit, where a short coast phase is performed, then the Centaur stage is restarted<sup>[3]</sup>. The tangential velocity of the Cape Canaveral Air Station is approximately  $v_0 = 0.4084 \text{ km/s}$ , while Earth’s escape velocity is  $v_{esc} = 11.1861 \text{ km/s}$ , leading to  $\Delta V_{esc} = v_{esc} - v_0 = 10.777 \text{ km/s}$ .
- **MCC2 X-1 Burn:** The S/C starts a burn to modify its trajectory on January 5, 1996. Analyzing the telemetry extracted by NASA Horizons, the manoeuvre is performed between 0:00:00 and 7:30:00. For this manoeuvre,  $\Delta V_{burn} = 0.0310 \text{ km/s}$ .
- **Insertion:** The S/C reaches the target halo orbit on February 14, 1996. Analyzing the telemetry extracted by NASA Horizons, the manoeuvre is performed between 16:21:00 and 17:51:00 with an overall  $\Delta V_{inj} = 0.0040 \text{ km/s}$ .
- **Trim manoeuvre:** The S/C starts a correcting manoeuvre to fix the halo orbit on March 20, 1996. The before mentioned telemetry shows that it happens between 23:30:00 and 0:30:00 of the following day. The estimated  $\Delta V_{trim}$  is approximately  $\Delta V_{trim} = 7.8 \text{ m/s}$ .

The Mission, not considering the fuel used for attitude corrections, has an overall  $\Delta V_{tot} = 10.820 \text{ km/s}$ . This result is coherent with the estimation of  $\Delta V_{budget} = 13.391 \text{ km/s}$  showed before. Even subtracting the budget allocated for attitude control (approximately  $43 \text{ m/s}$ ),  $\Delta V_{budget} > \Delta V_{tot}$ , demonstrating the accountability of the launcher. The result obtained even though non exactly correct, is considered by the team as consistent, given the lack of available data and the fact that this estimation is done in the early stage of mission analysis.

## 2 Propulsion Subsystem

### 2.1 Mission Analysis

The propulsion subsystem is designed to maintain the expected trajectory in the L1 Lagrangian point, to insert the S/C into the halo orbit and to perform the necessary manoeuvres of attitude control and station keeping.

To assure the success of the SOHO mission, a  $\Delta v$  budget was allocated following the phases presented in the list below; a detailed subdivision of the budget of the preliminary phases of the mission can be found in Table 4.

#### 2.1.1 Preliminary mission trajectory design

- **Launch and early orbit:** To achieve the desired trajectory, SOHO was launched with an Atlas II-AS from the *Spaceport Florida Launch Complex 36* into a circular parking orbit with an inclination of  $28.8^\circ$ . At time Launch+84 min, the ignition of the Centaur engine marked the end of the coasting phase in the parking orbit. Using the  $\Delta v$  provided by the Centaur, SOHO began the Transfer Trajectory Insertion manoeuvre (TTI). At time TTI+35 min, Centaur detached from the spacecraft.
- **MCC1 Burn:** The S/C starts to modify its trajectory. The manoeuvre was performed with two different burns, to provide initial assessment about the performance of the thrusters.
- **MCC2 Burn:** The second mid-course correction manoeuvre wasn't initially expected to be done during the preliminary analysis, but was then decided to use the manoeuvre to not simply correct the trajectory, but also to perform a shape change of the trajectory in order to reduce the necessary  $\Delta v$  budget of the halo insertion.
- **Halo insertion:** The S/C reached the target halo orbit on February 14, 1996. The preliminary analysis provided a  $\Delta v$  budget going from  $3.1 \text{ m/s}$  to  $12.7 \text{ m/s}$  depending on the date of the burn. The manoeuvre was performed on the February 14 given the low cost.
- **Trim manoeuvre:** The S/C started a correcting manoeuvre to fix the halo orbit on March 20, 1996.

The following tables resume the allocated and the effective  $\Delta v$  budget for the SOHO mission; the data have been taken from reference<sup>[31]</sup>. Due to the absence of information about the margin taken for each manoeuvre, the data are presented as found:

Manoeuvre	$\Delta v$ budget
MCC1	30
MCC2	30
HOI	122
TRIM	18
Station keeping	30
Attitude manoeuvres and Margin	45
Total	275

Table 4: Budget expectations<sup>[9]</sup>

Manoeuvre	True $\Delta v$ [m/s]
TTI	3200
MCC1	4.92
MCC2	31.7
HOI	3.1
TRIM	0.89
Total	3240.61
Total w/o TTI	40.61

Table 5: True  $\Delta v$

### 2.1.2 $\Delta v$ budget justification and retrieval

In order to compute the  $\Delta v$  budget consumed during the mission, the team computed the trajectory propagation of the S/C using MATLAB, by solving a three body problem in Cartesian form without considering perturbations such as J2 or the presence of the Moon. The procedure was the following:

1. Selection of the initial conditions for the state of each body, which are initial position and velocity of both Earth and spacecraft.
2. Compute, using a proper function, the first derivative of the states of Earth and S/C. For the gravitational pull acting on the Earth we considered the action of the Sun alone, while for the S/C the team accounted both the Earth and the Sun action.
3. The system is then propagated using the MATLAB function “ode113”.

If compared with the theory, this function proved to be quite effective, given proper initial conditions and options (such as the integrating time-step). Nevertheless, the system demonstrated to be quite unpredictable and sensible to the initial conditions selected: this forced the team to find a viable path through a trial and errors process. To keep the procedure as simple as possible, it was decided to find a mission plan that included just two manoeuvres: one impulsive burning for departure from the parking orbit, necessary to escape Earth gravity trough a quasi-parabolic trajectory, and one impulsive manoeuvre for inserting into the halo orbit around L1.

In the following tables is presented the comparison between the real data of SOHO’s manoeuvres and the data computed by simulating its trajectory. In particular Table 5 shows the  $\Delta v$  manoeuvres performed by the real S/C, and Table 6 the data achieved by the team. Both data do not consider the budget given by the launcher to reach the parking orbit.

Manoeuvre	Computed $\Delta v$ [m/s]
TTI	3231.0
HOI	969.8

Table 6: Computed  $\Delta v$

	True $\Delta v$ [m/s]	Computed $\Delta v$ [m/s]
Total	3240.61	4200.8

Table 7: Total True/Computed  $\Delta v$

As seen in the tables, the great discrepancy from the true data is given by the manoeuvre to insert into the halo orbit, caused by the simplicity of the model used, in which there is no presence of correction manoeuvres to reduce the budget of the orbit insertion.

In Figure 5 is shown the propagated trajectory using MATLAB as described.

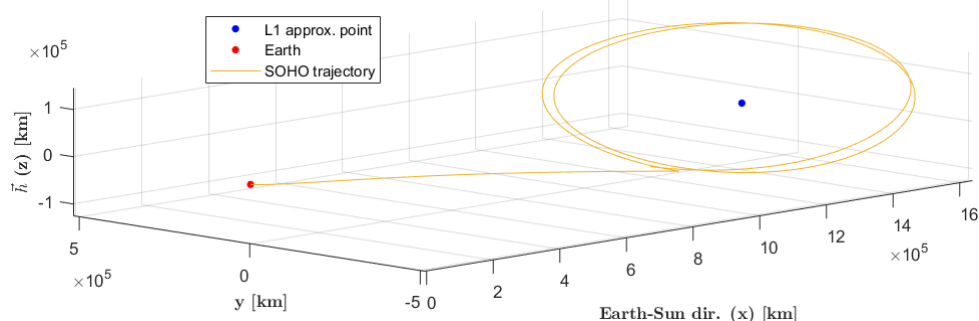


Figure 5: Computed trajectory

## 2.2 Subsystem Description

### 2.2.1 Architecture

The architecture of the propulsion subsystem can be summarized as shown in Figure 6.

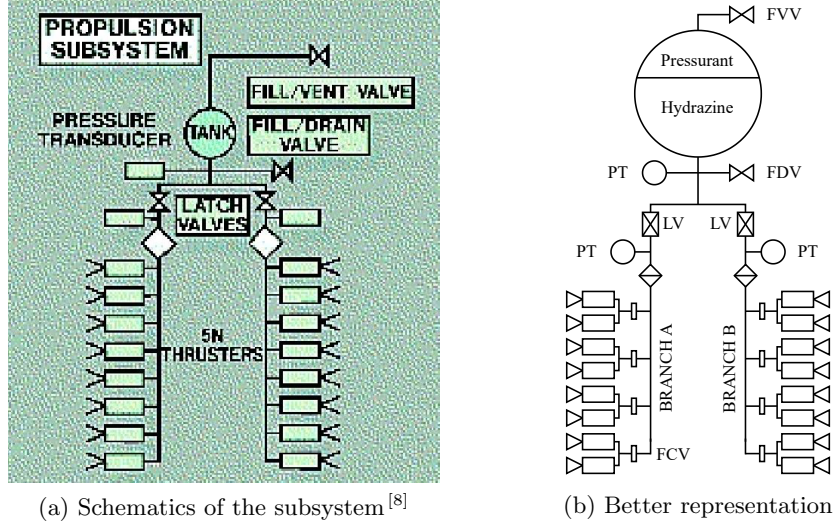


Figure 6: SOHO - blow-down architecture

The whole system can be represented through a *blow-down* architecture<sup>[32]</sup>: the tank, storing hydrazine and pressurant, is accessible thanks to the two valves called *Fill/Vent Valve* (FVV) and *Fill/Drain Valve* (FDV) while the pressure can be checked with *Pressure Transducers* (PT). Proceeding downstream, the *Latch Valves* (LV) allow to completely close one or both branches, called “Branch A” and “Branch B”, to separate the different parts of the system; one of them is responsible for the thrusters group from 1 to 4 while the other one for the group 5 to 8, as can be seen in Figure 6.

The *Dual Thruster Modules* (DTM) have a relatively stable thermal environment in the halo orbit and the temperature variations expected during the life time are related to the solar constant variation and degradation of the thermal optical properties of the external surfaces. The inclined thrusters - DTM 1 and 2 - are partially Sun illuminated, DTM 3 and 4 are always in the shadow of the spacecraft and DTM 5 to 8 are exposed to the Sun. Due to the stable environment, the thrusters thermal control is mostly achieved by a multi-layer insulation (MLI), and also a heater is mounted on the *Fuel Control Valve* (FCV) to cope with the cold environmental conditions. Figure 7 shows the DTM’s placement on the spacecraft:

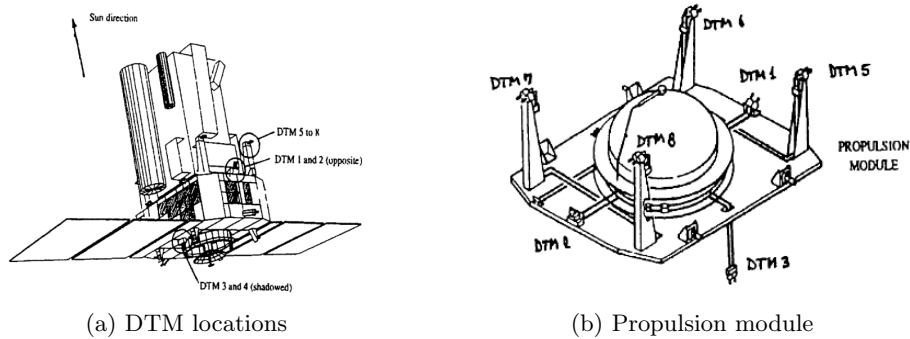


Figure 7: SOHO - propulsion module<sup>[2]</sup>

The equipped thruster model is *MRE-1.0* by *Northrop Grumman Corporation*, a hydrazine monopropellant thruster with a thrust range between 3.4 and 5 N, with a weight of 0.5 kg<sup>[18]</sup>. The 16 thrusters are actually organized in 8 DTM, of which four (5 to 8) are located on masts mounted on the upper platform of the service module, two are located directly on the upper platform and the last two are on the bottom side of the spacecraft, while the tank is mounted in its central cylinder; the pairs 1 and 2 are inclined 30° upwards, to limit plume impingement effect on the payload.

A key feature of the SOHO propulsion system is the coupling of the roll, pitch and yaw control loops through *parasitic torques*. These are unwanted torques generated during thrusting (e.g., a  $\Delta v$  in the z direction, applying torque about the x-axis), which also affect the other two axes; they occur because the thrusters are not mounted along orthogonal axes, and this causes attitude-pointing errors to grow in the control loop until they exceed a fixed limit, requiring a correction manoeuvre to be performed.

$\Delta v$ Direction	$-X$	$+X$	$-Z$	$+Z$
#DTM used	1 / 2	3 / 4	5 / 6	7 / 8
Parasitic Torque Axis	$Y$ (pitch)	$Z$ (yaw)	$X$ (roll)	$X$ (roll)

Table 8: Desired  $\Delta v$  Direction - Used DTM - Parasitic Torque Axis<sup>[10]</sup>

### 2.2.2 $\Delta v$ breakdown

Until the trim manoeuvre, the spacecraft operated the following manoeuvres:

Manoeuvre	Date	#DTM used	Planned $\Delta v$ [m/s]	True $\Delta v$ [m/s]	Fuel used [kg]
MCC1 <sub>1</sub>	03/12/95	1,2	4.66	3.04	2.59
MCC1 <sub>2</sub>	03/12/95	1,2	not done	1.878	1.6
MCC1 <sub>3</sub>	not done	7,8	0.34	not done	not done
MCC2 <sub>1</sub>	05/01/96	7,8	15.7	15.7	13.34
MCC2 <sub>2</sub>	05/01/96	7,8	10	10	8.46
MCC2 <sub>3</sub>	05/01/96	1,2	6	6	5.05
HOI	16/02/96	1,2	3.1	3.1	2.6
TRIM	20/03/96	1,2	0.89	0.89	0.75

Table 9: Manoeuvres until trim<sup>[11]</sup>

Table 10 collects the station keeping manoeuvres up to 2 years after the trim:

Manoeuvre	Date	#DTM used	Planned $\Delta v$ [m/s]	True $\Delta v$ [m/s]	Fuel used [kg]
SK-1	23/05/96	1,2	0.3067	0.3089	0.3353
SK-2	11/09/96	1,2	0.4541	0.4578	0.4925
SK-3	14/01/97	1,2	0.0432	0.0411	0.049
SK-4	11/04/97	1,2	0.1887	0.1892	0.2064
SK-5	04/09/97	1,2	1.8876	1.8972	2.0258
SK-6	29/11/97	3,4	0.0396	0.0408	0.0345
SK-7	19/12/97	1,2	0.3984	0.3956	0.4263
SK-8	17/04/98	1,2	1.4375	1.435	1.5441

Table 10: Station keeping manoeuvres<sup>[12]</sup>

## 2.3 Structural sizing

### 2.3.1 Propellant selection and margins

The starting point for the propulsion subsystem's sizing is the  $\Delta v$  budget. In the case of the SOHO mission, the budget allocated at launch was  $275 \text{ m/s}$ <sup>[32]</sup>. To this value, a 10% margin is added, totaling the starting value for  $\Delta v$  to  $302.5 \text{ m/s}$ .

Using the Tsiolkovsky equation shown in Equation (3), the mass ratio can be calculated:

$$MR = \frac{m_0}{m_f} = e^{\frac{\Delta v}{I_{sp}g_0}} = 1.1505 \quad (3)$$

where  $I_{sp} = 220 \text{ s}$  is the specific impulse of hydrazine and  $g_0 = 9.81 \text{ m/s}^2$ .

As the total mass at launch of the satellite is known to be  $m_0 = 1850 \text{ kg}$ , both the propellant mass  $m_{prop}$  and the dry mass  $m_f$  can be calculated solving Equation (4):

$$\begin{cases} m_f = m_0/MR = 1608.1 \text{ kg} \\ m_{prop} = m_0 - m_f = 241.95 \text{ kg} \end{cases} \quad (4)$$

As per MAR-MAS-040<sup>[33]</sup>, a 20% margin is added to the dry mass bringing the total to  $m_f = 1929.7 \text{ kg}$ . Regarding the propellant mass, a 2% margin for propellant residuals should be accounted as per MAR-MAS-080<sup>[33]</sup>; moreover, a 3% margin to take into account ullage and a 0.5% one for loading uncertainty are considered, thus ending up with a total propellant mass of  $m_{prop} = 255.26 \text{ kg}$ . Comparing it to the real mass of propellant that was loaded at launch, equal to  $251 \text{ kg}$ , a  $4 \text{ kg}$  difference can be noted: this discrepancy is most likely due to a difference in the margins applied to the propellant mass and possible uncertainties during loading.

Hydrazine has been chosen as propellant due to its convenient properties. First of all, it is stable and guarantees high performances with large thrust (ideal for station-keeping and control manoeuvres), avoiding both decomposition inside the tank and sensitivity to shocks; furthermore, it is stored as a liquid and it has a lifetime compatible with the whole mission ( $> 12 \text{ yrs}$ , considering that the mission has been designed for  $2 + 6 \text{ yrs}$ ). Its potential limit is the corrosivity of the exhaust gas, but a proper selection of the thruster (specifically hydrazine-designed) solves this issue.

The volume of the propellant can be computed given its density  $\rho_{prop} = 1010 \text{ kg/m}^3$ :

$$V_{prop} = \frac{m_{prop}}{\rho_{prop}} = 0.2527 \text{ m}^3 \quad (5)$$

Adding a 10% margin, as per MAR-CP-010<sup>[33]</sup>, the propellant volume becomes  $V_{prop} = 0.2780 \text{ m}^3$ .

### 2.3.2 Pressurant selection and sizing of the feeding system

As the hydrazine needs to be pressurized during the mission, a blow-down pressurisation system is implemented using helium as pressurant gas (light and inert). The blow-down system is chosen due to its simplicity and reliability with monopropellants (although it presents pressure and thrust decay in time and mass flow variation). To compute the blow-down coefficient  $B$ , the *Beginning-of-Life* (BOL) and the *End-of-Life* (EOL) pressures of the thrusters have been selected as the initial and final gas pressures respectively. Therefore, with  $P_{gas,i} = 22.4 \text{ bar}$  and  $P_{gas,f} = 6.6 \text{ bar}$ <sup>[32]</sup>, the blow-down coefficient is calculated as:

$$B = \frac{P_{gas,i}}{P_{gas,f}} = 3.3939 \quad (6)$$

This result is slightly lower than the typical values for this coefficient (usually  $B \simeq 4 \div 6$ ), but this can be explained considering that neither the pressures represent exactly the initial

and final conditions of the system: in fact, the EOL is a condition in which the thruster is still functioning, but can only produce the minimum possible thrust, thus the final pressure in the tank could be lower than the one defined for the thrusters in this condition. Similar analysis can be done for the BOL, where a higher tank pressure could be needed considering the losses given by the feeding system. Having calculated  $B$ , the initial volume of the pressurizing gas can be obtained:

$$V_{gas,i} = \frac{V_{prop}}{B - 1} = 0.1161 \text{ m}^3 \quad (7)$$

Considering helium to be a perfect gas, the ideal gas law can be used to compute the maximum pressurant mass required by the system. This is defined using the initial gas conditions  $P_{tank,i} = 22.4 \text{ bar}$  and  $V_{gas,i} = 0.1161 \text{ m}^3$  and the helium specific gas constant  $R_{He} = 2077.3 \text{ J/(kg K)}$ , while the gas temperature is estimated to be equal to the tank's one, defined as  $T_{tank} = 293 \text{ K}$ :

$$m_{press} = \frac{P_{tank,i} V_{gas,i}}{R_{He} T_{tank}} = 0.4274 \text{ kg} \quad (8)$$

A 20% margin is added as per MAR-MAS-090<sup>[33]</sup>, leading to the final value  $m_{press} = 0.5129 \text{ kg}$ .

### 2.3.3 Tank sizing

Necessary part of the propulsion subsystem is the tank, which needs to be sized according to the data found so far. A single tank is used, containing both the helium and the hydrazine. The starting point for tank sizing is the total volume, which can be computed as the sum of the initial pressurizer and propellant volumes:

$$V_{tank} = V_{gas,i} + V_{prop} = 0.3941 \text{ m}^3 \quad (9)$$

To this value, a 1% margin is added to account for bladder volume, so  $V_{tank} = 0.3981 \text{ m}^3$ . The real tank used on-board of the satellite is the *80263-1 propellant tank* by *Northrop Grumman Corporation*<sup>[34]</sup>. The volume of this tank is  $0.4612 \text{ m}^3$ . The discrepancy with the one calculated can be explained by noticing that this is the smallest tank capable of containing the computed volume, among the ones produced by Northrop Grumman.

The tank is made of titanium Ti-6Al-4V<sup>[35]</sup>, with a density  $\rho_{tank} = 4430 \text{ kg/m}^3$ , a tensile strength  $\sigma = 950 \text{ MPa}$  and it is shaped as an oblate spheroid. As a first approximation for sizing, a spherical shape is considered and the radius is calculated as:

$$R_{tank} = \left( \frac{3}{4} \frac{V_{tank}}{\pi} \right)^{\frac{1}{3}} = 0.4563 \text{ m} \quad (10)$$

This result is comparable to the dimensions of the real one oblate spheroid ( $1021 \text{ ID} \times 808 \text{ mm}$ )<sup>[34]</sup>. As it can be seen, the diameter of the computed sphere is close to the mean between the previously mentioned dimensions. The thickness of the tank can be computed from the maximum pressure that has to be sustained (the initial and higher gas pressure  $P_{tank,i} = 22.4 \text{ bar}$ ):

$$th_{tank} = \frac{P_{tank,i} R_{tank}}{2\sigma} = 0.538 \text{ mm} \quad (11)$$

Finally, the mass of the tank can be computed:

$$m_{tank} = \frac{4}{3}\pi\rho_{tank}((R_{tank} + th_{tank})^3 - R_{tank}^3) = 6.2444 \text{ kg} \quad (12)$$

This result is quite different from the real mass of  $34.5 \text{ kg}$ <sup>[34]</sup>. This could be due to a variety of reasons, mainly:

- **Higher security factor:** The operating pressure is around  $22 \sim 23$  bar, which means that the pressure the tank needs to withstand without yielding must be at least twice that pressure. To do that, a higher thickness is required.
- **Production problems:** The production of a titanium tank so thin could be problematic, especially considering the fact that it wasn't produced with modern technologies as it had to be built before 1995. This means that an higher thickness was required for the tank to be produced without the risk of instabilities.
- **Different mass count:** The datasheet does not specify how the total weight of the tank was calculated, so it is not known if external parts of the tank are considered (e.g. locking mechanism that helps attaching the tank to the spacecraft's structure, valves or pipe attachments). All of these elements have not been considered during the previously shown tank sizing and cannot be computed without further data.

#### 2.3.4 Mass budget

A fundamental parameter that characterises each subsystem is the mass budget; it can be computed as the sum of the masses required by the subsystem, in this case the tank's mass, the propellant's mass (both calculated during sizing) and the 16 thrusters' masses:

$$m_{PS} = m_{tank} + m_{press} + 16 * m_{thruster} = (6.2444 + 0.5129 + 16 * 0.5) \text{ kg} = 14.7573 \text{ kg} \quad (13)$$

Finally, a 10% margin is added to take into account cables' mass, leading to the complete mass budget  $m_{PS} = 16.2330 \text{ kg}$ .

#### 2.3.5 Power budget

To provide a power budget, the power required by each thrust valve (taken from the datasheet<sup>[18]</sup>) is considered, being  $P_{thrust} = 15 \text{ W}$  at  $28 \text{ V}(DC)$ . By multiplying this value taking into account all the 16 thrusters, the power budget is computed:

$$P_{PS} = 16 * P_{thrust} = 240 \text{ W} \quad (14)$$

#### 2.3.6 Final configuration

Table 11 sums up the values computed during the sizing (with margins) and the corresponding real data (whether found):

	Estimated values	Real data	Discrepancy
Propellant mass	255.26 kg	251 kg	+1.7%
Propellant volume	0.2780 m <sup>3</sup>	N/A	-
Pressurant mass	0.5129 kg	N/A	-
Tank volume	0.3981 m <sup>3</sup>	0.4612 m <sup>3</sup>	-13.7%
Tank dimensions	Sphere 456.3 mm radius	Oblate spheroid 1021 ID × 808 mm	-
Tank mass	6.2444 kg	34.5 kg	-81.9%
Mass budget	16.2330 kg	N/A	-
Power budget	240 W	N/A	-

Table 11: Comparison between sizing and real data

### 3 TTMTTC subsystem

Change log	
Paragraph number	Nr of the pages changed; nr of the tables/figures changed; 1 row per paragraph; short description of the change applied
3.1.1	(pp. 16); 1 value updated in the instruments data rates table
3.1.3	(pp. 16); 1 paragraph, better explanation on data rate computations
3.3.1	(pp. 18); 1 paragraph, rewrote losses (sizing) for better understanding
3.3.2	(pp. 18); 2 tables, updated results
3.3.3 - 3.3.5	(pp. 19 - 20); Entire sub sections, rewrote the signal to noise ratio equations as values and assumptions were incorrect; summed up all results in single table at the end for easier visualisation

The TTMTTC subsystem is divided into ground and space segments. It provides a link to transmit both scientific and telemetry data from S/C to ground and vice versa.

#### 3.1 Architecture

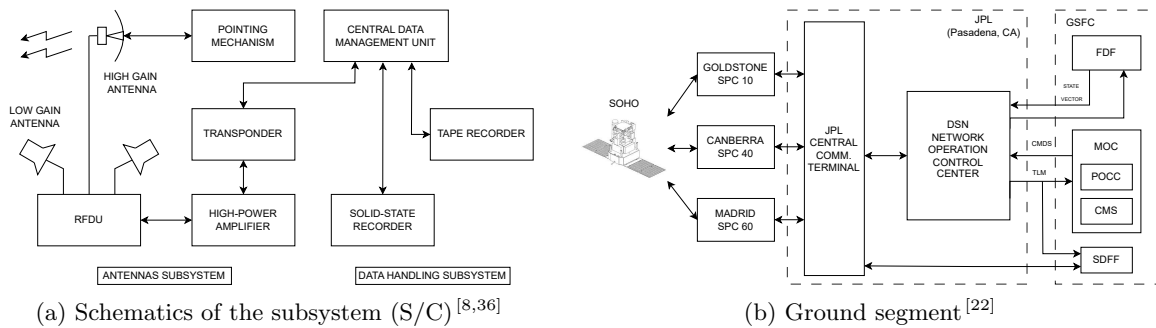


Figure 8: SOHO - TTMTTC architecture

As can be seen from the Figure 8 the subsystem can be divided in two main branches: one responsible for data storage and one devoted to data transmission.

##### 3.1.1 TTMTTC components

We can analyze all the system, including the data storage, describing also how the S/C can operate autonomously for 48 hours<sup>[36]</sup>:

- **Central Data Management Unit:**

The CDMU is responsible for: data acquisition and transmission to the ground, decoding and distribution of commands to all users.

- **Tape Recorder & Solid State Memory:**

With a capacity of 1 Gbit for the tape recorder and 2 Gbit for the solid state memory, this storage is mainly dedicated to registering telemetry and scientific data during operations without ground contact and for granting redundancy to the data handling subsystem.

- **High Power Amplifier:**

A High Power Amplifier (HPA) provides the 10 W output levels (in its high power mode) needed by the antenna during transmission.

- **High Gain Antenna:**

The HGA is a 804 mm reflector antenna having a gain of 22.7 dBi. It is made of a carbon fiber reflector, an aluminum feed cone (with a crossed dipole feed) and a reflective disk on top. The HGA operates in the S-band, right and left handed circular polarization for uplink and downlink respectively.

- **Low Gain Antenna:**

Two Low Gain Antennas (LGA), with a gain of -31 dBi, ensure omni-directional coverage. Used only for low rate telemetry, the two LGAs are *quadrifilar helix* antennas mounted in a way to have them to be resonant. They are installed on the + and - Z side of the spacecraft. Each LGA operates in S-band right handed circular polarization for both uplink and downlink. The antenna pattern is quasi-rotationally symmetric and quasi isotropic in the region of elevation between 0 and 108.5° considering the antennas' reference frame.

Table 12 presents data rate information per instrument:

<b>Payload</b>	<b>Data rate</b> [kbit/s]	<b>Payload</b>	<b>Data rate</b> [kbit/s]	<b>Payload</b>	<b>Data rate</b> [kbit/s]
GOLF	0.128	LASCO	4.2	VIRGO	0.1
SWAN	0.2	MDI/SOI	5 - 165	CELIAS	1.5
SUMER	10.5	COSTEP	0.3	CDS	12
ERNE	0.7	EIT	1	UVCS	5

Table 12: Instruments data rates<sup>[13,14]</sup>

### 3.1.2 Modulation & encoding

SOHO spacecraft utilizes a standard encoding to protect the data transmitted from errors, the Reed-Solomon (R-S) is applied to data packets of 1279 bytes (for downlink data, interleaved to a depth of five) and also a convolutional encoding is employed to better protect the data from errors<sup>[13]</sup>.

### 3.1.3 Transmission and Ground stations

SOHO transmits data in S-band: 2.2-2.29 Ghz is used for downlink, while 2.025-2.11 Ghz is adopted for the uplink. Furthermore, the data are streamed using duplicated receivers and transmitters.

The total data is carried with a bitrate ranging from a minimum of 1.19 kbit/s up to 219.6 kbit/s, results obtained as the sum of the max output from payloads (165 kbit/s<sup>[13]</sup>) and the telemetry data (54.6 kbit/s<sup>[14]</sup>).

Considering all the payloads to be active and an MDI data rate of 5 kbit/s, the instruments generate up to 40.628 kbit/s of data (from Table 12). During standard operations, the data rate transmitted is 95.228 kbit/s, obtained considering the housekeeping data (54.6 kbit/s<sup>[14]</sup>) and the data rate of the payload previously computed (40.628 kbit/s). Meanwhile, during the max usage mode of MDI, the data rate of the payload is dedicated all to this single instrument (165 kbit/s), resulting in the maximum data rate of 219.6 kbit/s.

NASA Deep Space Network (DSN) is providing T&TC support using existing ground station facilities in Madrid (Spain), Canberra (Australia) and Goldstone (CA, USA) and a central communications terminal at JPL. S/C operations are being performed by the *SOHO Mission Operations and Control Center* (SMOCC) at NASA/GSFC.

### 3.2 Mission phases correlation

SOHO is designed to operate in a **normal mode** in which the nominal routine operations are conducted; furthermore, in order to preserve the spacecraft from any possible damage or loss, a **safe mode** (Emergency Sun Reacquisition Mode) is possible. They can be described from the TTMTTC subsystem's viewpoint<sup>[37]</sup>:

- **Normal Mode:** During routine operations, the High Gain Antenna can be pointed at Earth, providing a high rate downlink of telemetry received by the 26-meter antennas. The nominal operating scenario, schematized in Figure 9, is designed as follows<sup>[14,22]</sup>:
  - 8 consecutive hours during which real-time communication is conducted with the ground stations (MDI high data rate at 160 kbit/s). This period is chosen to be day-light in NASA Goddard Space Flight Center and to overlap about half time with the US western and Canary Islands observatories<sup>[3]</sup>.
  - Three “silence” periods of 3.73 hours each, during which data is recorded on-board and no telecommunication with the ground segment is performed.
  - Three periods of 1.6 hours each between every silence period, in which real-time communication with the ground occurs and the data previously recorded is transmitted to the ground.

Whenever there is data transmission, the basic science data (40 kbit/s) is available with a small delay at the *Experiment Operation Facility* (EOF).

Furthermore, every year, for a period of two months (June and July, arbitrary selected<sup>[3]</sup>), SOHO is in continuous contact with the DSN for helioseismology data return.

- **Emergency Sun Reacquisition Mode:** During safe mode, the position of the Sun is approximately sensed to point the solar panels toward it for power supply; ground segment can provide control to stabilize the spacecraft. HGA cannot be used (no pointing to Earth is available) and the vital telecommunication with the ground is handled by the omnidirectional LGA, which is only capable of low rate telemetry transmission (no science data available) with the 26 meters stations. Using the LGA, medium rate telemetry transmission is only possible with 34-meter stations, while high rate telemetry only with 70-meter stations<sup>[37]</sup>.

SOHO mission is designed with three main phases (LEOP, TTP and HOP) in which the TTMTTC subsystem carries out different activities<sup>[22]</sup>.

1. **Launch and Early Operations Phase:** During launch, the High Gain Antenna is rigidly attached to the spacecraft. No telemetry or telecommunication with the ground is performed until the separation from the Centaur upper stage.
2. **Transfer Trajectory Phase:** Short time after the separation from Centaur (about 4 minutes), acquisition of telemetry begins with a delay of approximately three minutes and the telecommunication with NASA DSN is handled by the Low Gain Antennas; the High Gain Antenna is deployed after 8 hours and 20 minutes from separation. Completed these “preliminary” operations, the Normal Mode is activated, starting the routine operations.
3. **Halo Orbit Phase:** routine operations in Normal Mode.

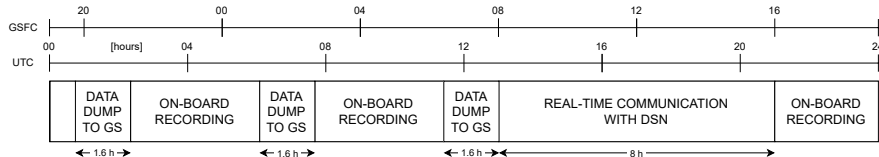


Figure 9: Normal Mode routine operations - 24 hours<sup>[3]</sup>

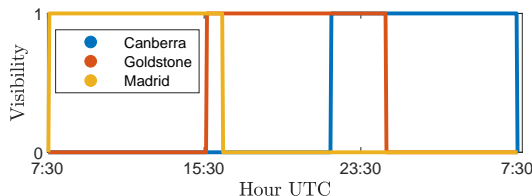


Figure 10: SOHO visibility - 24 hours

The Figure 10 has been modelled through GMAT<sup>[38]</sup> and MATLAB and it represents the visibility of the SOHO S/C throughout a single day (March 16<sup>th</sup> 1996). Visibility data can be obtained by modelling Ground Stations and trajectory of S/C in GMAT (1 when visible, 0 otherwise). It can also be noted a 30 minutes shadow with no visibility (c.a 7 am - 7:30 am).

### 3.3 Sizing

#### 3.3.1 Losses

The losses that need to be taken into consideration are: cables, atmospheric, free space and pointing. The worst case condition is considered: maximum distance of  $r_{max} = 1,768,767 \text{ km}$  and a total cable loss of  $L_{cab} = -3 \text{ dB}$  (as no data is available, the generic range  $-1 \div -3 \text{ dB}$  is considered). The atmospheric loss is obtained from the graphical approximation<sup>[39]</sup>.

The pointing and the free space losses can be computed from the following equations, where  $\eta_{point}$  is the pointing accuracy,  $\lambda$  the wavelength and  $D$  the diameter of the receiving antenna:

$$\begin{cases} L_{point} = -12 \left( \frac{\eta_{point}}{\theta_{rx}} \right)^2 \text{ [dB]} \\ \theta_{rx} = 65.3 \frac{\lambda}{D} \end{cases}$$

$$L_{free} = 20 \log_{10} \left( \frac{\lambda}{4\pi r_{max}} \right) \text{ [dB]}$$

The parameters used for the computation and the resulting losses are summed up in Tables 14 and 15.

#### 3.3.2 Antennas

Both HGA and DSN antennas are parabolic antennas, so their efficiency can be approximated as  $\mu = 0.55$ . For both uplink and downlink, the gain can be computed:

$$G = 10 \log_{10} \left( \frac{\pi^2 D^2 \mu}{\lambda^2} \right) \quad (15)$$

where  $D$  is the diameter of the antenna (26 m for DSN and 0.804 mm for HGA). The calculated gains are compared with the real ones<sup>[14,40]</sup> in Table 13. As it can be seen, the computed values are similar to the real ones. The difference can be attributed to the antenna efficiency that does not perfectly reflect the one of the real antenna.

<b>Uplink</b>			<b>Downlink</b>		
	Computed	Real		Computed	Real
$G_{tx-DSN} \text{ [dB]}$	52.4186	51.4	$G_{tx-HGA} \text{ [dB]}$	22.9397	22.7
$G_{rx-HGA} \text{ [dB]}$	22.2242	22.7	$G_{rx-DSN} \text{ [dB]}$	53.1340	51.4

Table 13: Antenna gains for uplink and downlink

Moreover, the system noise density can be computed for both antennas as  $N_0 = 10 \log_{10}(k \cdot T_s)$  where  $k = 1.380649 \cdot 10^{-23} \text{ J/K}$  is the Boltzmann constant and  $T_s$  is the temperature of the receiving antenna (21 K for DSN and 250 K for HGA). The results are  $N_{0-DSN} = -215.3770 \text{ dB}$  and  $N_{0-HGA} = -204.6198 \text{ dB}$ .

### 3.3.3 Link budget equation

The link budget can now be computed: having defined the *BER*, the minimum value of the *Energy per bit per Noise density*  $E_b/N_{0,min}$  can be obtained knowing that the transmission is Reed-Solomon encoded and modulated through BPSK; to this, a +3 dB safety factor is added for both downlink and uplink. As no specific data is available on the *Bit Error Rate* (*BER*) used, the most common values are considered:  $10^{-5}$  for the downlink and  $10^{-7}$  for uplink, where the difference between the two values comes from the fact that commands sent from the GS require an higher accuracy.

Equation (16) is used to compute the  $E_b/N_0$  which has to be compared with the minimum value:

$$\begin{cases} \frac{E_b}{N_0} = P_{tx} + G_{tx} + G_{rx} + L_{total} - N_0 - 10 \log_{10}(R) \quad [\text{dB}] \\ P_{tx} = 10 \log_{10}(P_{tx} [\text{W}]) \quad [\text{dB}] \\ L_{total} = L_{free} + L_{point} + L_{atm} + L_{cab} \quad [\text{dB}] \end{cases} \quad (16)$$

The total losses  $L_{total}$  and the datarate  $R$  vary over time depending on the distance: the worst case scenario is considered, with maximum datarate ( $R_{max} = 219.6 \text{ kbps}$  as computed in Section 3.1.3) at maximum distance (the one used for free space losses calculations).  $P_{tx}$  is the transmission power converted in dB. The resulting values and the parameters used are summed in Tables 14 and 15.

As expected, both uplink and downlink receivers are capable of receiving the signal, distinguishing it from the noise.

### 3.3.4 Signal to noise ratio

To compute the Signal to noise ratio, the carrier power must be firstly retrieved. This can be done through Equation (17), where  $P_{mod, loss}$  is the carrier modulation index reduction obtained from the modulation index  $\beta_{mod}$  estimated to be  $60^\circ$ , considering normal-mode bit rates.

$$\begin{cases} P_{mod, loss} = 20 \log_{10}(\cos(\beta_{mod})) \\ P_{carrier} = P_{rx} + P_{mod, loss} \end{cases} \quad (17)$$

Given the fact that the bandwidth  $B$  used during the design phase of the mission cannot be retrieved, an estimation has to be made, considering a roll-off factor of  $\alpha = 0.574^{[41]}$ . Then, the carrier signal to noise ratio  $SNR_{carrier}$  can be obtained as shown in Equation (18).

$$\begin{cases} B = R(1 + \alpha) \\ SNR_{carrier} = P_{carrier} - N_0 - 10 \log_{10}(B) \end{cases} \quad (18)$$

From this, the  $SNR_{margin}$  can be computed as the difference between the  $SNR_{carrier}$  value found and the minimum one (approximated at  $SNR_{min} = 10 \text{ dB}$  as the transmission is between the spacecraft and the DSN antennas) to check that the receiver is capable of tracking the signal, distinguishing it from the noise.

The results are summed in Tables 14 and 15; as it can be seen for both cases the condition on  $SNR_{margin}$  is not respected. This is probably due to some approximations and estimations that had to be done during this analysis: as most of the data regarding SOHO's TTMTTC subsystem was not readily available, generic values were used. However, during the development of the

mission, values different from the general case ones were probably taken as they were the most suitable to solve specific problems that we were not able to predict and consider.

### 3.3.5 Results

The following tables present the parameters used and the results obtained for the HGA antenna:

	<b>Uplink</b>	<b>Downlink</b>
$\lambda [m]$	0.1450	0.1335
$D [m]$	0.804	26
$\eta_{point} [deg]$	0.1	0.01
$\theta_{rx} [deg]$	11.78	0.34
$P_{tx} [dB]$	17.7815 <sup>[42]</sup>	10 <sup>[14]</sup>
$E_b/N_0,min [dB]$	11	9
$P_{carrier} [dB]$	-140.35	-147.42

Table 14: Parameters

	<b>Uplink</b>	<b>Downlink</b>
$L_{free} [dB]$	-223.7	-224.4
$L_{point} [dB]$	-8.6520e-4	-0.0107
$L_{atm} [dB]$	-0.04	-0.04
$L_{cab} [dB]$	-3	-3
$E_b/N_0 [dB]$	16.88	20.56
$SNR_{carrier} [dB]$	8.89	12.57
$\left(\frac{E_b}{N_0}\right) > \left(\frac{E_b}{N_0}\right)_{min} + 3 dB$	✓	✓
$SNR_{margin} > 3 dB$	✗	✗

Table 15: Results

## 4 AOCS subsystem

Change log	
Paragraph number	Nr of the pages changed; nr of the tables/figures changed; 1 row per paragraph; short description of the change applied
4.1.2	(pp. 22 - 23); 1 paragraph, formatting changes and better description of Gyro C. Clearer illustration of overall AOCS functioning, Sensors and Actuators
4.2.1	(pp. 24); 1 paragraph, reformulation of part of the Normal Mode. New references added
4.2.3	(pp. 25); 1 paragraph, reformulation of parts of pointing budget
4.3.1	(pp. 26); 2 paragraphs, better description of the SRP with results
4.3.2	(pp. 26 - 27); Whole sub chapter, all changed from ground up, better results discussion
4.3.3	(pp. 27 - 28); 2 paragraphs and 2 tables, changes to results description and better page layout

The *Attitude Orbit Control System* (AOCS) subsystem needs to guarantee adequate knowledge of the position and attitude of the spacecraft at all times. Moreover, it shall guarantee correct pointing of the sensors, thrusters, solar array and antenna during all phases of the mission, with an accuracy which is dependent on the specific case.

### 4.1 Architecture

#### 4.1.1 Overview

SOHO is a 3-axis stabilized spacecraft with a Sun-pointing stability of 1 *arcsec* over a period of 1.5 minutes in nominal conditions<sup>[36]</sup>. The AOCS provides the satellite with the means to<sup>[13]</sup>:

- accurately point the scientific instruments towards the Sun
- control the roll angle around the Sun-pointing axis
- perform orbit manoeuvres

In the reference frame, the positive X-axis is pointed along the Sun direction, the Z-axis points towards the northern celestial sphere and the Y-axis completes the right-handed orthogonal triad. The roll angle is controlled to fix the spin axis of the Sun in the XZ body plane: this imposes a roll that ranges from -7.25 deg and +7.25 deg over the course of a year, while the S/C completes an orbit around the Sun<sup>[11]</sup>. This is also confirmed by the spin axis of the Sun being tilted of 7.25 deg with respect to the axis of the Earth's plane of ecliptic<sup>[43]</sup>.

This behaviour is needed so that the scientific instruments can always have the same orientation with respect to the Sun, providing consistent results during operations (e.g. GOLF sensor, monitoring solar velocity's oscillations). Another motivation can be found in passive attitude stability but, since disturbances appear to be low, it is less relevant.

#### 4.1.2 Sensors and Actuators

Table 16 and Table 17 summarise the components used by AOCS (see Table 1 of “*The SOHO Spacecraft*”<sup>[44]</sup>):

Sensor Type	Number	Direction
Rate Integrating Gyro	3	+X
Star Sensor	2*	+Z
Fine Pointing Sun Sensor	2*	+X
Sun Acquisition Sensor	3*	+X, +Z, -Z

Table 16: Sensors

\* including redundant components

Actuator Type	Number
Reaction Wheel	4
Thruster	16

Table 17: Actuators

The core of the AOCS is the *Inertial Reference Unit* (IRU) composed of the three roll rate-integrating gyros, the *Star Sensor Unit* (SSU) with two star trackers, two *Fine Pointing Star Sensors* (FPSS) and three *Sun Acquisition Sensors* (SAS). Two set of eight thrusters and four reaction wheels are used as actuators. During normal scientific operations, yaw and pitch are measured by the FPSS (**Z** and **Y** axis rotations respectively, see Figure 11), and the roll is measured by the SSU (**X** axis rotation, Figure 11), while the gyros are not required, and are only used for thruster-based manoeuvres such as RW unloading, *Emergency Sun Reacquisition* (ESR) and *Initial Sun Acquisition* (ISA).

**Gyros:** the three gyros (all oriented along the +X direction, Table 16) are assigned to perform the following functions<sup>[45]</sup><sup>[46]</sup>:

- **Gyro A:** connected to *Fault Detection Electronics* (FDE) for roll-rate measurements for ESR (see Section 4.2.1) using thrusters
- **Gyro B:** connected to FDE for excessive roll-rate anomaly detection
- **Gyro C:** connected to *Attitude Control Unit* (ACU) for roll attitude during computer-based control modes using thrusters

It is pointed out how **Gyro C** is the only one measuring directly the roll angle and connected to the ACU, therefore the other two are not used for nominal attitude control, but rather for calibration manoeuvres or recovery sequences, commanded and executed under ground operator control<sup>[46]</sup>. However, all gyros are intended to be fully active during momentum-management manoeuvres. Because of their intrinsic nature, they also need to be periodically calibrated to correctly determine the drift bias associated with measurements.

**SSU:** they work by first identifying a guide star, then mapping the field of view and processing the data using a multi-star-identification algorithm<sup>[11]</sup>. They're directed toward +Z, as can be seen in Figure 4 of “*The Solar and Heliospheric Observatory (SOHO) Mission: An Overview of Flight Dynamics Support of the Early Mission Phase*”<sup>[11]</sup>; their position and orientation is justified by the star availability constraint, and is also crucial to avoid the extreme radiation coming from the Sun, that can damage the devices or reduce their visibility on the rest of the stars. They have an accuracy of 1 *arcsec*, and they are produced by *Leonardo Company*<sup>[47]</sup>.

**FPSS:** they are produced by *Redwire* and have a field of view of  $\pm 4.25^\circ \times \pm 4.25^\circ$  and an accuracy of 15 to 20 *arcsec*<sup>[48]</sup> each; they're all oriented towards +X because in nominal conditions that is the direction of the Sun with respect to the S/C.

**SAS:** of the three mounted, two have line of sight in the +Z and -Z direction, while the third points towards the +X direction; this arrangement guarantees omni-directional coverage, and permits a preliminary coarse alignment of the spacecraft towards the Sun during ISA (see Section 4.2), before switching to fine Sun pointing.

**RW:** the four reaction wheels are arranged symmetrically in a pyramidal configuration about the X-axis<sup>[11,37]</sup>, as can be seen in Figure 4 of “*The Solar and Heliospheric Observatory (SOHO) Mission: An Overview of Flight Dynamics Support of the Early Mission Phase*”<sup>[11]</sup>. Since the attitude can be controlled with three RW, the fourth wheel is held in reserve. Also, having multiple RW helps to bear the momentum needed for the control, both increasing components expected lifetime and making saturation events less frequent (occurring when it reaches maximum spin velocity, supplying a zero net torque). Each reaction wheel has a momentum storage of 40 Nm, and they are produced by *Bradford Engineering*<sup>[49]</sup>.

**Thrusters:** they are organized in 8 pairs of hydrazine engines (Dual Thrust Module, DTM). At the L1 point, the main environmental disturbance is the Solar Radiation Pressure, whose resulting torque is compensated by the reaction wheels, that need to be periodically unloaded with the use of thrusters; the mission requires this unloading to be executed not sooner than 8 weeks<sup>[22]</sup>, in conjunction with the station keeping of the halo orbit. The unloading is accomplished using the spacecraft’s ACU computer.

#### 4.1.3 Redundancy

It is remarkable to note that the number of sensors and actuators exceeds the number of components effectively needed: this is due to redundancy, implemented to overcome faults that can otherwise compromise the mission. In fact, the gyroscopes can be removed and still make the satellite work properly: in theory, the SSU alone can provide the complete attitude of the S/C, even if the FPSS (which is not able to determine the roll attitude) is still useful to verify the pointing error towards the Sun.

In 1998, a series of ground errors led to a major loss of attitude and subsequently of the gyros<sup>[45]</sup>, but once the connection was restored, ESA and NASA were capable of installing a new “gyroless” control software to manage the attitude without the faulted components<sup>[36,37]</sup>.

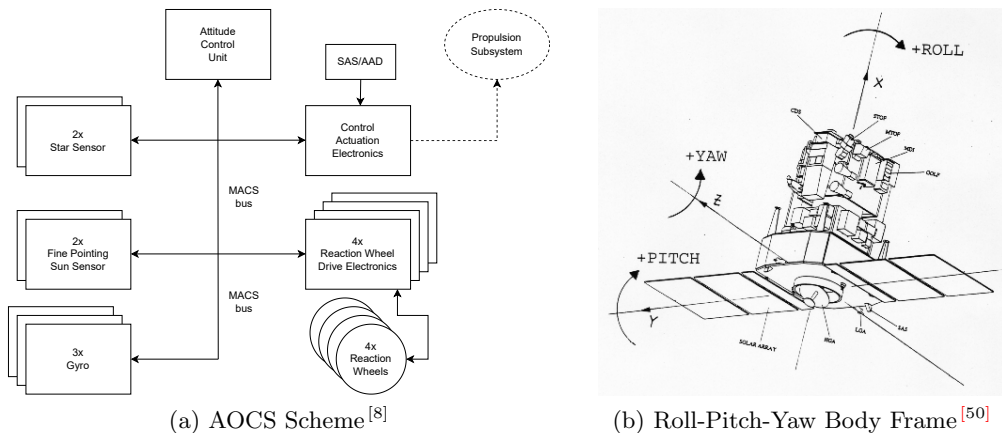


Figure 11: SOHO - AOCS architecture

## 4.2 Control Modes and Correlations

### 4.2.1 Control Modes

During the mission, SOHO has to adapt to different requirements in terms of pointing accuracy and stability, hence the need of four different control modes, one for standard operations and three for particular cases that may arise.

**Normal Mode (NM):** In Normal Mode the science data collection is performed<sup>[46]</sup>, therefore the +X axis (see Figure 11), that corresponds to the payloads' optical axis, must be directed towards the Sun. It is also possible to point the *High Gain Antenna* (HGA) towards the Earth, providing communications with ground station: this is made possible because the SOHO's orientation is fully known by the sensors, and the HGA can be steered in the planet direction<sup>[37]</sup>.

The attitude control is performed by spinning up or slowing down the four reaction wheels, positioned into pyramidal configuration<sup>[36]</sup>. Their control input is computed by the *Attitude Control Unit* (ACU), using the data coming from the *Fine Pointing Sun Sensor* and one of the SSU<sup>[37]</sup>. The “roll steering law” dictates the movement of the stars in the star tracker to keep SOHO perfectly aligned with the Sun's North-South axis.

Reaction wheels are employed in this mode because of their precision and effectiveness: these are controlled with electric power and, for this reason, are more versatile than thrusters as their use is not limited by the total fuel mass stored. Another aspect to point out is the *minimum impulse bit* (MIB), which is the smallest control torque that can be provided by the thrusters: basically absent in reaction wheels, it allows for a more precise control.

**Emergency Sun Reacquisition (ESR) Mode:** This mode ensures the survival state of the spacecraft in case of major anomalies<sup>[46]</sup>. In ESR Mode, the S/C attitude is controlled entirely by onboard hardware, the *Fault Detection Electronics* FDE, separated from the ACU that senses the approximate position of the Sun and makes use of thrusters to autonomously ensure pointing towards the Sun<sup>[37,51]</sup>; furthermore, in this emergency mode, the ground segment is able to control the reaction wheels to adjust the pointing.

The choice of the autonomous use of thrusters (and not of the reaction wheels) in ESRM lies in the greater reliability of the firsts, which do not even face saturation issues and also in the fact that the thrusters grant a more robust feedback compared to the RW; the employment in ESR Mode also can justify the large redundancy in the number of thrusters.

A pointing precision of 2 degrees limits the “error box” of the ESR Mode. Communication with ground is established with an omnidirectional Low Gain Antenna (the HGA is not available in ESR Mode since it cannot be pointed towards Earth) which exchanges information with the ground control<sup>[37]</sup>.

The Emergency Sun Reacquisition Mode can be triggered by two different sensors, called *Fine Sun Pointing Attitude Anomaly Detector* (FSPAAD) and *Coarse Sun Pointing Attitude Anomaly Detector* (CSPAAD), which enable the ESR Mode when they detect the Sun to be outside a 5-degree or 25-degree radius circle respectively<sup>[36]</sup>. Regarding the accuracy, a 5-degree pointing error is chosen as a sufficiently large threshold to be unambiguously attributed to a fault, but low enough to require a limited control action. Considering the 25-degree error, it has been chosen as a large enough “safe range” in case of Fine SPAAD failure.

When ESR Mode is triggered, an update is sent to onboard instruments, since some of them are sensible to minimal deviations from the nominal attitude (e.g. LASCO instrument can overheat if not properly oriented) or suffer contamination from the thrusters (e.g. CDS, SUMER, CELIAS)<sup>[37]</sup>. Some instruments are capable of modifying their configuration in order to preserve the sensitive sensors: LASCO, for example, is able to adjust “front aperture doors” and “shutters”<sup>[52]</sup>.

**Initial Sun Acquisition (ISA) Mode:** The ISA Mode is designed to perform the initial Sun acquisition operation, which is preliminary before the Nominal Mode and, also, it is performed after the ESR operations. The aim of this mode is to point the S/C towards the Sun by computing the attitude from the Sun-sensor and performing the pointing manoeuvre with the A-branch of thrusters. The employment of thrusters is justified in this operation considering that no fine Sun-pointing is required, since it is a preliminary operation before the beginning of the Nominal Mode, in which a finer Sun-pointing is then performed.

**Roll Maneuver Wheels (RMW) Mode:** In this configuration SOHO's attitude is determined by making use of the FPSS and the star tracker. During this mode, strict alignment with Solar north-south is not maintained because RMW mode is used for thrust manoeuvres of station keeping and momentum management; the last manoeuvre is necessary to unload the reaction wheels when they reach a certain threshold, or to speed up the wheels in order to maintain the operative speed in a certain range to increase stability. This operation is necessary due to the nature of the reaction wheels; they must work under a specific threshold and above a certain value of rpm to maintain operational stability.

#### 4.2.2 Correlation with phases

The main phases of the SOHO mission are LEOP (Launch and Early Orbit Phase), TTP (Transfer Trajectory Phase) and HOP (Halo Orbit Phase). The nominal operations performed by the Normal Mode occur from the beginning of the TTP and go on during the HOP, while during the LEOP different event-driven operations are carried out. After the lift-off and before the separation from the launcher's upper module (Centaur), attitude data are acquired by Centaur. After the separation, when the power is still supplied by batteries, AOCS is activated and ISA is performed. Then, once the solar arrays have been deployed, AOCS is re-initialized (because of the new S/C configuration), ISA is once again performed and finally Normal Mode is executed<sup>[14]</sup>.

#### 4.2.3 Pointing Budget

The pointing budget of the Attitude and Orbit Control Subsystem is dictated by the accuracy requirements of the onboard scientific payloads. Regarding the absolute performance error (APE), a pointing precision of  $5 \text{ arcmin}$  is required for the scientific payload alignment with the Sun, while  $15 \text{ arcmin}$  is set for the roll angle; furthermore, the scientific instruments' Sun-alignment has to be at least  $1 \text{ arcsec}$  in the short term (15 minutes) and  $10 \text{ arcsec}$  in the medium term (6 months)<sup>[13]</sup>. The roll angle's pointing precision is respected using star sensor with error within  $1 \text{ arcsec}$ , while the instruments' Sun-alignment requirements are satisfied using the FPSS, which has an error of  $15 \div 20 \text{ arcsec}$ . The requirements are dictated not only by scientific objectives, but also by the Thermal Control Subsystem. In fact, it has been studied<sup>[4]</sup> that due to the thermo-elastic effect each instrument could be subject to progressive misalignment with the FPSS, so the pointing budget allocated for the payloads previously described is deeply affected by this. The thermal control has been considered has a main driver for the pointing budget since SOHO does not face periods of eclipse, being continuously exposed to the Sun. **In addition to the AOCS inputs, the gyros' drift bias has to be considered.**

Regarding the other subsystems, it can be noticed that the only element that can be rotated independently from the S/C is the High Gain Antenna (Telecommunication Subsystem), which has a pointing budget of  $\pm 32 \text{ deg}$  that allows communication with the ground segment performing an Earth pointing<sup>[13]</sup>; this can be justified by the fact that SOHO must be able to exchange communication with the GS during its entire nominal orbit, so a wide pointing budget for the HGA is desired.

On the other hand, both the Propulsion Subsystem (thrusters) and the Power Subsystem (solar arrays) are fixed to the S/C, so they do not have their own pointing budget. Furthermore, solar arrays are almost always pointed towards the Sun (due to the geometry of the S/C), without getting into eclipses or shadow.

### 4.3 Sizing

The sizing of the ADCS is fundamental to estimate the energy and fuel consumption of a S/C during its station keeping activities and pointing. Furthermore, it is needed to define the required configuration for both sensors and actuators.

### 4.3.1 Disturbances

The *Solar Radiation Pressure* (SRP) was modelled in order to estimate the most significant disturbance torque; meanwhile, other disturbances such as *Gravity Gradient* (GG) and *Magnetic field*, were not considered since their contribution is negligible if compared to the SRP. *Aerodynamic drag* is basically not existing. This can be explained since the S/C is located 1.5 mln Km away from the Earth and at 1% of the *average Earth-Sun distance*.

The contribution of SRP can be evaluated as:

$$T_{srp} = \frac{F_{s(L1)}}{c} A_s (1 + q) \cos(I) (C_{sp} - C_g) = 5.7280 \cdot 10^{-6} \text{ Nm} \quad (19)$$

where  $F_{s(L1)} = 1394.8 \text{ W/m}^2$  is the solar intensity measured at L1,  $c$  is the speed of light,  $A_s = 9.5 \times 2.7 \text{ m}^2$  is the area exposed to the Sun<sup>[53]</sup> (the one connected to the solar panels),  $q = 0.6$  is the reflectivity coefficient,  $I$  is the relative angle between the incoming rays and the surface (considered to be 0 to account for worst case condition) and finally  $C_{sp} - C_g = 0.03 \text{ m}$  is the considered lever arm between SRP and the center of mass of the satellite. These data have been chosen within typical ranges.

A 100% margin is applied to the disturbance torque to account for uncertainties, leading to  $T_{dis} = (1 + 1)T_{srp} = 1.1456 \cdot 10^{-5} \text{ Nm}$ .

### 4.3.2 Modelling

As SOHO mounts a set of 4 reaction wheels and a set of 16 thrusters, the latter are used when wheel saturation occurs or whenever their unloading is necessary. We start by computing the total angular momentum that must be compensated for a single orbit:  $h_{1orb} = T_{dis} \cdot T_{orb} = 176.1853 \text{ Nms}$ , where  $T_{orb}$  is the orbit period (equal to about 178 days<sup>[8]</sup>).

The inertia matrix of the S/C has to be computed; SOHO is considered to be a  $4.3 \text{ m} \times 3.7 \text{ m} \times 2.7 \text{ m}$  parallelepiped (X, Y and Z respectively;  $4.3 \text{ m} \times 9.5 \text{ m} \times 2.7 \text{ m}$  with solar arrays unfolded)<sup>[53]</sup>. Not knowing the exact inertia matrix, the team decided to overestimate the inertia considering the unfolded configuration. For the worst case scenario the maximum principal inertia is taken:  $I_{max} = M/12 \cdot (4.3^2 + 9.5^2) = 1.6764 \cdot 10^4 \text{ kg m}^2$ , considering the wet mass  $M = 1850 \text{ kg}$ . It can be seen that  $I_{max}$  corresponds to  $I_{zz}$  (slew manoeuvres will be considered to be performed around this major axis).

**Reaction wheels** Given the maximum angular momentum<sup>[49]</sup>  $h_{max,rw} = 40 \text{ Nms}$  that the reaction wheels can store, it is possible to calculate the maximum time they can be used before reaching saturation:

$$\begin{cases} n_{orb,sat} = \frac{h_{max,rw}}{h_{1orb}} = 0.2270 \text{ orbits} \\ t_{max,before-sat} = n_{orb,sat} T_{orb} \approx 40 \text{ days} \end{cases} \quad (20)$$

As expected, the obtained value of 40 days is far less than  $T_{orb}$ , thus the wheels will need to be unloaded multiple times per orbit by firing the thrusters. It can be noted that the obtained value is coherent to the real time occurring between two consecutive saturations of the wheels (approx. 8 weeks<sup>[54]</sup>).

Considering a slew manoeuvre, the worst case is set to be a  $\theta_{slew} = 180 \text{ deg}$  rotation. Since we know the maximum torque of the reaction wheels<sup>[49]</sup> to be  $T_{max,rw} = 0.248 \text{ Nm}$ , we can compute the minimum time  $t_{min}$  for which the slew manoeuvre can be performed and consequently the maximum angular velocity  $\dot{\theta}_{slew}$  at which the manoeuvre can be executed:

$$\begin{cases} t_{min} = \sqrt{\frac{4\theta_{slew} I_{max}}{T_{max,rw}}} = 921.6563 \text{ s} \\ \dot{\theta}_{slew} = \theta_{slew}/t_{min} = 0.1953 \text{ deg/s} \end{cases} \quad (21)$$

**Thrusters** The same slew maneuver can now be analyzed with the thrusters, imposing a manoeuvre of  $\theta_{slew} = 180 \text{ deg}$  and a *triangular* thrust profile (simplest and most common): considering both accelerating and decelerating firings to happen one after the other, thus not considering a “costing phase” in which the S/C is left to inertial kinematics. Again, we compute the minimum time  $t_{min}$  required to perform the slew manoeuvre and consequently the propellant mass (hydrazine,  $I_{sp} = 220 \text{ s}$ ) needed:

$$t_{min} = \sqrt{\frac{4 I_{max} \theta_{slew}}{n L F_{thr}}} = 75.4560 \text{ s} \quad m_{prop,slew} = \frac{2 n F_{thr} t_{slew}}{I_{sp} g_0} = 1.3985 \text{ kg} \quad (22)$$

where  $n = 4$  thrusters (2 DTM are used, Section 4.1.2) and considering that each thruster can provide a thrust<sup>[18]</sup> of  $F_{thr} = 5 \text{ N}$ .

A remark on the choice of  $L$ : the slew manoeuvre is performed around  $I_{zz} = I_{max}$ , so the 2 couples of thrusters can be fired in the x-direction ( $L = 4.3/2 \text{ m}$ ) or in the y-direction ( $L = 3.7/2 \text{ m}$ ); although for the computation of the inertia  $I_{max}$ , a simplified model with the SA unfolded has been considered (so, with dimension  $9.5 \text{ m}$  instead of  $3.7 \text{ m}$ ) in reality the dimension of  $9.5 \text{ m}$  can not be used for the thrusters’ placement since it’s only related to the solar arrays’ wingspan. For this reason, the original dimensions of  $4.3\text{m} \times 3.7\text{m} \times 2.7\text{m}$  have been considered and the worst case scenario for the selection of  $L$  has been taken into account, leading to  $L = 3.7/2 \text{ m} = 1.85 \text{ m}$ .

Reaction wheels are often used for their simplicity and benefit of working with electric power: they don’t require fuels or additional materials but they need to be unloaded every time the maximum angular acceleration is met. Thrusters can be used for this, and we can compute the minimum time required for the de-saturation, considering  $n = 4$  thrusters for 1 reaction wheel:

$$t_{des,min} = \frac{h_{max,rw}}{n L F_{thr}} = 1.0811 \text{ s} \quad m_{prop,des} = \frac{t_{des} F_{thr}}{I_{sp} g_0} = 0.0025 \text{ kg} \quad (23)$$

### 4.3.3 Results

Apart from the actuator chosen, the slew maneuver has been implemented for a  $180 \text{ deg}$  rotation, representing the worst case scenario. This operation can be done with both reaction wheels and thrusters, using electric power or fuel stored onboard. As the propellant is a finite resource and must be used as smartly as possible, the reaction wheels will be preferred for attitude control manoeuvres. This means that the thrusters are used when the wheels need to be despun to avoid saturation. Moreover, they are also used during trajectory correction, as they can supply a net force that the RW cannot generate (given their ability to only apply torques).

The sizing revealed that RW, used for attitude correction while Sun pointing, need to be unloaded with thrusters every 40 days with a fuel consumption of  $0.0025 \text{ kg}$ . From the numbers computed, this correction will be performed approximately 5 times every orbit, considering a 178 days revolution around L1 (about 10 times per year).

The SOHO S/C is perfectly able to make a continuous pointing at the Sun, while keeping the antennas pointed at Earth to exchange data: the only attitude maneuvers are related to station keeping and small corrections (regarding attitude, not mentioning L1 trajectory insertion maneuvers). Orbiting around L1 allows to constantly point both the Sun (with the payloads) and the Earth (with the antennas). The amount of propellant used for desaturation is negligible compared to the total stored onboard at launch ( $m_{fuel} = 251 \text{ kg}$ ), therefore it is compliant to the nominal lifespan of the mission (2 years<sup>[13]</sup>).

**Power Budget** All the sensors and the actuators need to be powered through the electrical subsystem, so an analysis on the maximum power consumption can be done. Table 18 summarises the maximum power consumption for each of them.

**Mass budget** Moreover, an estimation on the mass of actuators and sensors mounted on the satellite can be done. Table 19 sums up the masses of each component. This doesn't take into account the propellant mass necessary for correction manoeuvres calculated before.

Reaction wheel	29 – 168 W each <sup>[49]</sup>
Thrusters valve	8.5 W each <sup>[18]</sup>
Star tracker	13 W each <sup>[47]</sup>
FPSS	0.7 W each <sup>[48]</sup>
Total	211.4 – 767.4 W

Table 18: Maximum power consumption

Reaction wheel	6.70 kg each <sup>[49]</sup>
Thruster	0.5 kg each <sup>[18]</sup>
Star tracker	7.2 kg each <sup>[47]</sup>
FPSS	2 kg each <sup>[48]</sup>
Total	53.2 kg

Table 19: Mass budget

In conclusion, data found through the reverse sizing reflects the real values associated with the SOHO mission. Moreover, it explains the choices on the position and type of sensors and actuators (as shown in Section 4.1 and Section 4.2). Moreover, it helps to explain the longevity of the mission, which was scheduled to last 2 years but is still on going, with still fuel to burn, as predicted when analysing the amount necessary to despin the wheels every orbit.

## 5 TCS subsystem

### 5.1 Architecture

The *Thermal Control Subsystem* (TCS) controls the temperature ranges both with passive and active thermal control solutions, in order to keep the components' temperature within precise ranges (Table 21) to avoid them to be damaged or severely compromised in their performances.

#### 5.1.1 Overview

The TCS of the SOHO S/C is divided in two main parts, as shown in Figure 12: the *Payload Module* (PLM) TCS, and the *Service Module* (SVM) TCS. These two parts are connected by an interface ring, which guarantees thermal decoupling between the two and so it must be treated as a separate component.

The TCS relies on both active and passive solutions for the SOHO spacecraft, because of the various scenarios that can be faced during the mission (Section 5.2): passive controls aim at controlling the temperatures with non moving parts and fixed configurations, while active elements can be controlled in order to change the thermal fluxes of the components.

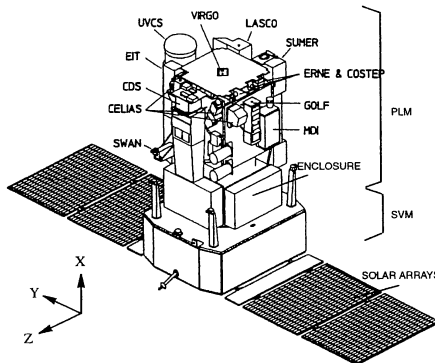


Figure 12: TCS Subdivision<sup>[4]</sup>

#### 5.1.2 Payload Module TCS

The major requirements that have to be guaranteed by the PLM TCS can be summarized as<sup>[13]</sup>:

- maintain the thermal conditions stable to meet all the pointing requirements of both the AOCS and the payload scientific experiments;
- guarantee a radiative environment acceptable for the scientific instruments;
- keep the equipment mounted on the PLM structure within acceptable temperature ranges.

To achieve this requirements the S/C employs different techniques for the various parts of the PLM structure:

- the external surfaces are covered with a *multi-layer insulation* (MLI) made of 13 layers of different materials: the outer layer utilizes carbon-filled Kapton, whereas for the inner layers either Mylar or Kapton are used;
- the internal surfaces are black painted, as to guarantee good and predictable radiative coupling and to minimize temperature gradients.

The PLM is in charge of the complete thermal control for all electronic units (except for MDI and LASCO electronics) and for the VIRGO unit. In fact, all the other experiment units perform their own thermal control: in this case, the PLM thermal control only guarantees their temperature reference point to be inside the requested range using appropriate heat sink temperatures. This also guarantees the proper radiative environment. Furthermore, the PLM controls the substitution heaters that are activated through duty cycle adjustment, when their associated experiment unit are not powered. All the sensors are connected to the structure through isostatic mounts that both isolate them from the S/C and guarantee the smallest possible thermo-elastic distortion.

As shown in Figure 12, the experiments' sensors are mounted on the upper lateral panels ( $\pm Z$  and  $\pm Y$ ) and on the upper panel ( $+X$ ) under the sunshield; all these panels are covered in MLI blankets.

Some instruments and some subsystem electronics are placed on the lower lateral panels ( $\pm Z$  and  $Y$ ), conductively decoupled from the upper panels. Their thermal control is performed by the S/C TCS in order to keep their temperature as close as possible to the panels one ( $20^{\circ}\text{C}$ ). This is done through the use of a single black Kapton sheet radiator that closes each of the 3 lower panel enclosures. The external faces use low emittance tape to adjust the thermal optical properties of these sensors.

The sunshield always faces the Sun ( $+X$  direction) and acts as a radiator for both the instruments and the electronics placed on it.

As shown in Figure 13, the outer layer is called *Optical Solar Reflector* (OSR) and is made of multiple tiles. To compensate for their aging and for the solar flux seasonal variation, heaters are placed on the rear side of the sunshield and are controlled by the TCS.

### 5.1.3 Service Module TCS

The SVM maintains thermal regulation through the implementation of an MLI blanket that surrounds its structure while leaving the radiators exposed. Various materials, such as Black Kapton MLI, Acheson Electrodag 501<sup>[55]</sup> and PSG120FD<sup>[56][57]</sup> paints, are employed for this purpose. To ensure uniform temperatures within the SVM, Chemglaze Z306<sup>[58]</sup> black paint is applied across all the surfaces except for the central cylinder (to reduce unwanted heat leaks to space, that would increase the required power)<sup>[4]</sup>.

This is done to minimize temperature gradients inside the module, that could lead to structural deformations (and failure in the worst cases). This is possible only because the components inside the SVM have similar working temperatures (Table 21), otherwise different solutions would have to be implemented.

### 5.1.4 Interface Ring

The decoupling between SVM and PLM is achieved through the use of an interface ring whose temperature is maintained at  $20^{\circ}\text{C} \pm 5^{\circ}\text{C}$  throughout the whole S/C lifetime. This is done to limit PLM deformation induced by the SVM<sup>[13]</sup>. Furthermore, this allows to split the thermal analyses between SVM and PLM, treating them as separate components, handled by different contractors<sup>[4]</sup>. Moreover, the separation introduced by this component allows to decrease the temperature gradient between the two parts; this configuration helps avoiding the insurgence of structural failure due to the high difference in temperature.

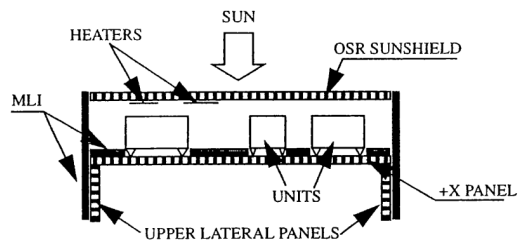


Figure 13: SOHO Sunshield Enclosure<sup>[4]</sup>

## 5.2 Mission phases correlations

SOHO's main mission phases are the *Launch and Early Operational Phase* (LEOP), the *Transfer Trajectory Phase* (TTP) and the *Halo Orbit Phase* (HOP). For every phase, a hot case and a cold case can be identified. For the TCS design, because of their analog configuration (i.e. with solar arrays deployed and the S/C pointing to the Sun) the TTP and HOP can be considered as single "nominal" phase decoupled from the LEOP. In fact, the active thermal control during LEOP is carried out by the launcher's upper stage Centaur<sup>[59]</sup> – suggesting that SOHO S/C shall only passively satisfy the thermal requirements of this phase –, while on TTP and HOP the thermal control is directly and solely in charge of SOHO's TCS.

**LEOP** Since the LEOP is characterized by operations conducted with the launcher's upper stage Centaur<sup>[59]</sup>, the active thermal control of the SOHO-Centaur system is not executed directly by SOHO. In this phase, the predominant environment is the Earth's one, with the albedo, the IR emissions and the solar irradiance as main thermal sources; since the internal components are turned on and off for early commissioning purposes, the team suggests that the internal heat source is not representative of this phase and, looking only at the in-orbit operations, identifies the cold condition in the parking orbit's eclipse and the hot condition in the parking orbit's sunlight period. In any case, this phase lasts about 80 minutes, so the time would not be enough to establish a steady-state thermal environment. The white painting (PSG120FD) covering the SVM has appositely been selected for its high emissivity/absorptivity ratio needed during this phase.

**TTP** The TTP begins after the separation from Centaur with the injection in the transfer trajectory towards L1. This phase begins with the deployment of the solar arrays, then the *Initial Sun Acquisition* (ISA) occurs (when the S/C starts to point at the Sun) and the components on-board are active. During the TTP there is a progressive change in the environment, passing from a planetary condition near the Earth (with albedo, IR emissions and solar irradiance) to L1 (with the solar irradiance becoming the predominant heat source).

**HOP** The halo orbit around L1 is the nominal environment of the mission and, since the point is located 1.5 million km from Earth, the solar irradiance is considered as the predominant source of heat<sup>[59]</sup>, while heat coming from Earth can be neglected. The thermal control is handled by the passive devices explained in Section 5.1 and by heaters for the payloads, since the temperatures of scientific instruments shall stay within a specific range and may require heating when non operating. It can be noted that parts of the S/C are partially shadowed by the solar arrays, while other parts are completely shadowed, for example the High Gain Antenna which always points to the Earth: the TCS handles this temperature gradient too.

## 5.3 Sizing

### 5.3.1 Spacecraft modelling

In first approximation, the sizing of the spacecraft's thermal control has been modelled through a mono-nodal analysis, with total S/C area equal to the main body surface  $A_{S/C} = 2(l_1 \cdot l_2 + l_1 \cdot l_3 + l_3 \cdot l_2)$  and a "cross section" equal to  $A_{cross} = 9.855m^2$ , which is the surface facing both the Sun and the Earth due to the S/C shape and positioning; the solar panels' surface has not been taken into account because it does not contribute to the total heat flux of the S/C components.

These values along with other data used for the modelling are shown in Table 20.

Parameter	Value [-]	Parameter	Value [ $m^2$ ]	Parameter	Value [W]
$\varepsilon_{S/C}$ (MLI)	0.03	$A_{S/C}$	74.32	$Q_{int-max}$	933
$\alpha_{S/C}$ (MLI)	0.12	$A_{cross}$	18.58	$Q_{int-min}$	454

Table 20: SOHO thermal data<sup>[4]</sup>

Regarding the various ranges of temperature of SOHO, according to literature about the mission, all on-board instruments are designed to have a certain operating temperature that has to be maintained during the operations, as shown in Table 21:

Part	Component	Working temperatures [°C]	Part	Component	Working temperatures [°C]
SVM	Hydrazine Tank	-197 ÷ 650	PLM	ERNE	0 ÷ 3
	Hydrazine	2 ÷ 114		GOLF	17 ÷ 20
PLM	Interface Ring	20 ± 5		EIT	16 ± 2
	CDS	20 ± 2		LASCO	-80
	CELIAS	-2 ÷ 24		MDI	30 ± 2 and 17 ± 2
	COSTEP	-7 ÷ 11		SUMER	75
	SWAN	0 ÷ 30		UVCS	-7 ÷ 23

Table 21: Instruments temperatures<sup>[4,15]</sup>

### 5.3.2 Modelling

The following are the equations used for the sizing with the approximations explained before, where  $q$  represents the heat flux, whereas  $Q$  is the power considering different external shells of the S/C. The view factor was not modelled and it is considered to be unitary.

$$q_{Sun-S/C} = q_0 \left( \frac{R_{Earth}}{R_{S/C}} \right)^2 \left[ \frac{W}{m^2} \right] \quad (24)$$

$$q_{albedo-pl} = q_{Sun-S/C} \alpha \cos(\theta) \left( \frac{R_{pl}}{R_{orbit}} \right)^2 \left[ \frac{W}{m^2} \right] \quad (25)$$

$$q_{IR-pl} = \sigma \varepsilon T_{pl}^4 \left( \frac{R_{pl}}{R_{orbit}} \right)^2 \left[ \frac{W}{m^2} \right] \quad (26)$$

Above, the heat fluxes of Sun, albedo and infrared are shown. The exchanged powers can now be calculated with the following formulas, remembering to use the proper areas:

$$Q_{Sun-S/C} = A_{cross} \alpha q_{Sun,S/C} [W] \quad (27)$$

$$Q_{albedo-S/C} = A_{cross} \alpha q_{albedo,pl} [W] \quad (28)$$

$$Q_{IR-pl} = A_{cross} \varepsilon_{S/C} q_{IR,pl} [W] \quad (29)$$

The total balance of the nodal analysis can now be computed following the nodal equilibrium:

$$\sum_i Q_i^- = 0 \quad \sum_j Q_{absorbed,j} = \sum_k Q_{emitted,k}$$

The total balance, considering also heaters and radiators is:

$$Q_{internal} + Q_{Sun-S/C} + Q_{albedo-pl} + Q_{IR-pl} + Q_{heater} = Q_{emitted} + Q_{radiator} \quad (30)$$

Remembering that  $Q_{emitted} = \sigma \varepsilon A (T_{S/C}^4 - T_{deep\ space}^4)$ , Equation (30) can be inverted to solve for  $T_{S/C}$  with specific boundaries conditions.

### 5.3.3 Results

Given the generic formula for a single node preliminary analysis, the various critical scenarios can be analyzed by imposing the appropriate boundary conditions. A first approximation can be done considering no active or passive thermal control components, while their presence can be implemented later to ensure a safe temperature excursion.

A second approximation consists of excluding the temperature range of instrument such as LASCO and SUMER because, as seen in Table 21, they greatly differ from the others; this can be justified considering that both instruments have their own dedicated thermal control unit, so they can be safely ignored.

**Hot case - TTP** This first case analyses the S/C in the hottest part of its trajectory directed towards L1. Radiation emitted by the S/C and the produced power are considered as internal heat fluxes, whereas external heat fluxes are the Earth's albedo, Earth's infrared radiation and the heat generated from the Sun.

Given the fact that the temperature found in this scenario ( $127.5^{\circ}\text{C}$ , without radiators) exceeds the predetermined one, an additional passive cooling system must be added. The simplest solution is the use of radiators, whose required surface and dissipated heat power can be computed with the equation presented below:

$$Q_{generated} + Q_{IR-pl,@Earth} + Q_{Sun-S/C,@Earth} + Q_{albedo-pl,@Earth} = Q_{IR}^{out} + Q_{radiator} \quad (31)$$

With  $Q_{IR}^{out} + Q_{radiator} = Q_{emitted}$ . Considering a desired temperature of  $20^{\circ}$  (the higher value of Table 21, removing LASCO and SUMER), the following results are obtained:

Inward [W]				Outward [W]
$Q_{gen}$	$Q_{IR}^{in}$	$Q_{Sun}$	$Q_{albedo}$	$Q_{emitted}$
933	109.1	1617.2	596.5	3255.8

Table 22: Exchanged power hot case, TTP

The radiators required surface is  $6.52\text{m}^2$  and the dissipated heat power  $Q_{rad} = 2404.1\text{ W}$ .

**Cold case - L1** This second case can be defined as the configuration reached at the L1 destination. Here, the distance of the S/C from Earth is approximately  $1.5 * 10^6\text{ km}$ , whereas the one from the Sun is  $1.4810 * 10^8\text{ km}$ . The Earth's orbit radius used for the computation of the Sun heat flux is  $1.496 * 10^8\text{ km}$ .

The resulting analysis provide a temperature of  $86.03^{\circ}\text{C}$ . Even thought the case is considered as the cold one, the resulting temperature is collocated above the maximum one, making it necessary again for a form of passive cooling. The following formula describe the whole system:

$$Q_{generated} + Q_{IR-pl,@L1} + Q_{Sun-S/C,@L1} + Q_{albedo-pl,@L1} = Q_{IR}^{out} + Q_{radiator} \quad (32)$$

Following the same procedure of Section 5.3.3, the surface of the radiators is obtained, resulting in an area of  $3.28\text{m}^2$ .

Inward [W]				Outward [W]
$Q_{gen}$	$Q_{IR}^{in}$	$Q_{Sun}$	$Q_{albedo}$	$Q_{IR}^{out}$
454	0.002	1650.1	0.0112	2104.1132

Table 23: Exchanged power cold case, L1

The results obtained have not great significance in the sizing, given the absence of a true cold scenario with the necessity of an active heating system. For this reason a further case will be analyzed considering the coupling of the hot and cold cases of the mission.

**Coupled case** The coupled case can now be analyzed: both cold and hot configurations are computed in order to determine how the S/C will behave with a singular fixed configuration. The hot case is used to size the cooling radiators and their presence is used to propagate the effect on a different environment: a cold case sizing is then performed to reach a final configuration.

Area radiators [ $m^2$ ]	S/C temperature w/o heaters, cold case [°C]	$Q_{heat}$ [W]
6.52	1.75	541.4

Table 24: Coupled case results

The results obtained highlights the necessity of both a passive cooling system for the hot case, as already depicted in Section 5.3.3, but also the need of an active heating, to warm the S/C from the temperature shown in Table 24 to the desired one of 17°C.

### 5.3.4 Budget

From the data obtained, power consumption and mass estimation of both passive cooling and active thermal control was done. Considering the radiator panel, the density of a honeycomb aluminum structure for space application is around  $\rho_{rad} = 12 \text{ kg/m}^2$ , with a thickness of 23mm; the density of the MLI protection depends on the number of layers used and on the material: in this case we adopted a Kapton-based MLI with a density of  $1.2 \text{ kg/m}^2$ , with 13 layers. Heaters are typically made up of a thin resistive element protected between two layers of protective plastic material and do not carry significant weight. As no information regarding the data-rate of the thermocouples has been found, their sizing cannot be computed.

Component	Heaters	Radiators	MLI
Mass [kg]	~ 0	78.3	81.4
Power [W]	541.4	2404.1	851.7

Table 25: Thermal control budget

From the data presented, the total power computed for the heating of the spacecraft results higher than the effective mounted on SOHO, equal to 303 W<sup>[4]</sup>, which is likely due to the fact that the model for simplicity doesn't include the contribution of additional thermal insulation inside the spacecraft or the autonomous thermal control of instruments and other components inside the S/C. Regarding the mass computed for the passive cooling, the masses obtained are compatible in term of percentage of the dry mass of the S/C, with a value of 9.98%, with other mission found in literature with thermal requirements similar to SOHO<sup>[60]</sup>.

### 5.3.5 Conclusions

From the data collected during the sizing it can be noted how in both the hot and cold cases the S/C cannot operate without thermal control. Radiators are needed for the first one, while heaters are implemented for the other.

In both cases the configuration reached is similar to the real one, with the most important thermal architecture being the coupled case, where the fixed configuration is analyzed.

The sizing proved to be effective without the use of active thermal control solutions (e.g. louvres), validating the SOHO architecture.

## 6 EPS subsystem

### 6.1 Architecture

#### 6.1.1 Overview

The *Electrical Power Subsystem* (EPS) supplies the electrical energy required by the S/C in each phase of the mission, providing regulation, protection and distribution of an initial 1500 W coming from the solar arrays and two batteries. It goes without saying that it is fundamental, because every active device of the S/C relies on it to pursue its function.

The architecture of the EPS is summarized by Figure 14:

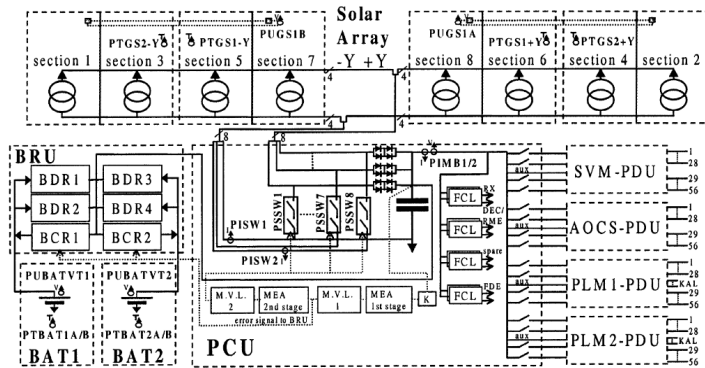


Figure 14: EPS Architecture with telemetry parameters (see Table 26)

#### 6.1.2 Power Management

**Power Control** The *Power Control Unit* (PCU) is responsible for the central power regulation, with a sequential switching shunt regulator and a  $2.2mF$  capacitor on the main bus, that acts as a voltage ripple eliminator; the main bus is always kept at a voltage of  $28V \pm 1\%$ <sup>[44]</sup>.

The power is distributed by 112 *Latching Current Limiters* (LCL), located in four *Power Distribution Units* (PDU), each with four buses separating main and redundant units, as well as heater circuits and electronic units; these LCL provide automatic switch-off during undervoltage (below  $23.5V$ <sup>[44]</sup>) events, thus protecting the system.

**Solar Arrays** The solar arrays are composed of two wings in the +Y and -Y direction<sup>[61]</sup>, each consisting of 2 solar panels and 1 yoke panel; each panel is divided electrically in two sections, and for each section there are four double strings, with *Back Surface Reflection* (BSR) silicon solar cells. Of these double strings, three have two cells in parallel and 77 cells in series, while the fourth has two cells in parallel and 78 cells in series<sup>[62]</sup>.

The SOHO trajectory around the Sun determines a fluctuation in Sun intensity of around 6%<sup>[16]</sup>; in the winter the spacecraft is closer to the Sun, leading to higher power produced by the solar arrays and less power consumed by the heaters, and of course the opposite situation happens during summer, that is the most critical point for power margins.

**Batteries** The two batteries are composed of 32 Ni-Cd cells, with a capacity of 20 Ah each. In nominal condition the batteries are never used, due to a permanent Sun-pointing configuration, and are kept fully charged by a trickle charge rate of  $90mA$ <sup>[16]</sup>; they will also keep slowly degrading over time, and can't be reconditioned for use in nominal condition, however they are used for transient consumption peaks or emergency situations (for example during the 1998 recovery<sup>[16]</sup>). This kind of batteries have a relatively low *Depth-of-Discharge* (DOD), their use is therefore justified by the small number of recharging cycles predicted in design phase.

Battery charge and discharge regulation is managed by the *Battery Regulator Unit* (BRU), controlled by the *Main Error Amplifier* (MEA) in the PCU, so that the excess solar arrays power can be used first for battery charging before being shunted.

### 6.1.3 Main parameters

For EPS monitoring and assessment, the major power subsystem telemetry parameters listed in Table 26 are used; these parameters are registered every 15 seconds, downloaded to the DSN ground stations and routed to the NASA GSFC in Greenbelt, where they will be analyzed and stored.

Name	Type	Description
PISW1	$I_{sc}$	Short circuit current, solar array section 1
PISW2	$I_{wp}$	Working point current, solar array section 8
PUGS1A/B	$V_{oc}$	Open circuit voltage
PTGS1+/-Y	$T_{ob}$	Temperature back side inner panels
PTGS2+/-Y	$T_{sh}$	Temperature back side outer panels
PSSW1-8	bi-level	Shunt section status: shunting or on-bus
PIMB1/2	$I_{load}$	Main bus current
PUBATVT1	$V_{bat1}$	Battery 1 voltage
PUBATVT2	$V_{bat2}$	Battery 2 voltage
PTBAT1A/B	$T_{bat1}$	Battery 1 temperature
PTBAT2A/B	$T_{bat2}$	Battery 2 temperature

Table 26: Telemetry parameters<sup>[16]</sup>

Before downloading to ground, the analogue measurements are converted to 8-bit parameters that guarantees a Least Significant Bit (LSB) of around 0.39% ( $1/2^8$ ) of the full acquisition range. For long-term performance evaluation, the daily averages of the last day of the month are used, except for specific min-max search purposes.

## 6.2 Mission phases correlations

The EPS architecture is necessary for the correct behaviour of the spacecraft and many on-board instruments require electric power to operate. For this reason, an analysis of all the electrically powered elements of SOHO is necessary to better understand its power budgets and requirements.

### 6.2.1 Power demands

In Table 27 and in Table 28 are listed all the power requirements for both the 12 payloads and for the subsystems.

Payload	Power [W]	Payload	Power [W]	Payload	Power [W]
GOLF	85.5	LASCO	68.5	VIRGO	14.3
SWAN	10.2	MDI/SOI	57	CELIAS	18.9
SUMER	37	COSTEP	25.8	CDS	58
ERNE <sup>[63]</sup>	7.1	EIT <sup>[64]</sup>	2.6	UVCS	36.9

Table 27: Payloads power requirements<sup>[17]</sup>

Regarding the spacecraft, the data presented are referred to the worst case scenario for each subsystem, in which the entirety of the components work in contemporary. An example of this can be made considering the combination of AOCS and Propulsion Subsystem, that in *Emergency Sun Re-acquisition* mode have a power demand of just 150 W<sup>[65]</sup>, compared to the maximum budget allocated for that subsystem. Also considering the propulsion unit, it is unrealistic that all the thrusters will operate at the same time, but if it is considered a manoeuvre of station keeping the power consumed is only 17 W<sup>[18]</sup>.

Subsystem	Power [W]	Subsystem	Power [W]
Propulsion	136	AOCS	181
TTMTC	107	TCS	303

Table 28: Subsystems power requirements<sup>[4,18,19]</sup>

The AOCS power consumption was retrieved, in first analysis, from the total power budget of the service module<sup>[4]</sup>, by subtracting to it the power demand of the telemetry<sup>[19]</sup> and the propulsion subsystems<sup>[18]</sup>.

### 6.2.2 Phases

**LEOP** During the initial phases of the mission, the power demand of SOHO was given principally by the telemetry subsystem, the ADCS subsystem and from the thermal control activity. The power is supplied by the two nickel cadmium batteries; in this phase begins also the deployment of the solar arrays which will power the S/C and recharge the batteries.

**TTP** During the transfer trajectory phase the spacecraft maintains the same power consumption as the previous phase, with a change in the power supply, that is now provided by the solar arrays.

**HOP** In the Halo orbit phase, the power consumption increases. This due to the fact that along the basic operation carried by the service module, in the primary phases of the halo orbit begins the calibration of the payload, so it was expected a variable electric demand based on the instrument calibrating. Completed the calibration of all the instruments, the operative phase begins, considered the more power demanding given the contemporary activation of multiple instruments and of the service module with all its subsystems.

### 6.2.3 Modes

Concerning the spacecraft operating modes, the power distribution significantly change between the two principal modes:

- **Normal mode:** the S/C power consumption is given by the sum of the thermal control, the AOCS subsystem and the TTMTC subsystem, with also a contribution given by the different payloads; note that not all the instruments work contemporary but only few at the time, depending on the telemetry budget spendable and on the scientific plan. The total power consumption computed by the data found in literature, is equal to 1029.8 W, of which 608 W consumed by the service module, and 421.8 W absorbed by the payloads.
- **Emergency Sun Re-acquisition mode:** during this mode the payloads are shut-off, and the respective protection are used for each instrument to prevent malfunctions; the only operative subsystems are the propulsion, the AOCS, the TTMTC and the thermal control one. As can be expected the power demand is much lower than when the spacecraft is in normal mode, resulting in a total of 560 W.

### 6.2.4 Considerations

Analyzing the Table 27, it can be immediately noticed that the most power demanding payloads are CDS and MDI: these two can be used to size the payloads consumption. The *SSA Data Archive*<sup>[66]</sup> has been used to gather information about the activity of the two most demanding payloads: as can be noticed by selecting a proper time interval (when both instruments are working) they do not work simultaneously, it appears that the MDI is the most frequent used payload between the two and it is shut down whenever the CDS is being used, to preserve power (see 10/4/2011, focus on 12:00).

This behaviour has been traced back to the overall maximum power consumption for the payloads, since there is not additional information on specific S/C attitude or vibration threshold for each payloads' working conditions that would otherwise justify this. Furthermore there is a small overlapping of the activity times: proving once more a power related behaviour.

Finally, the sizing criteria was found in the HOP phase (normal mode), since it is the most power-consuming with a total of 1029.8 W.

## 6.3 Sizing

During the nominal operations, the solar arrays are always pointed towards the Sun, with a designed power generation of 1500 W<sup>[13]</sup>, even though in Section 6.2.4 a smaller consumption was found. The batteries are only used in emergency cases where the power generation is not working, so their power output is lower as most power hungry components are shut down.

### 6.3.1 Solar Arrays

Because the solar arrays are always pointed towards the Sun, the time in eclipse  $T_e$  is assumed to be zero and the daylight time  $T_d$  is assumed to be the predicted lifetime of 2.5 years. To the power generated, a 20% increase must be included as per MAR-PWR-060<sup>[33]</sup>. The power requested to the solar arrays  $P_{SA}$  in order to satisfy the S/C demand can be computed from Equation (33), where the line efficiency in daylight  $X_d$  is assumed to be 0.8. This is a pretty safe assumption, as the panels were made specifically for the mission and with the precise objective of staying always exposed to the Sun, producing almost always maximum power.

$$P_{SA} = \left( \frac{P_e T_e}{X_e T_d} + \frac{P_d}{X_d} \right) = 2250 \text{ W} \quad (33)$$

The Sun irradiance at L1 can be computed from the one of the Earth (i.e. 1 AU) as the S/C is at 99% of the distance between the two celestial bodies:  $P_0 = P_{@1AU}/0.99^2 = 1384.6 \text{ W/m}^2$ .

To compute the specific power of the solar arrays, the efficiency of the Si-based cells must be defined. From the testing done before the launch, the resulting value is  $\varepsilon_{cell} = 13.4\%$ <sup>[62]</sup>. This is an assumption, as the real value can only be obtained once the S/C is operational. Moreover, solar flares and solar cycle events can affect the resulting value. Nonetheless, considering similar missions orbiting L1, the value obtained can be safely used, given that the percentage variation from the real condition can be estimated to be around  $\pm 1\%$ .

$$P_{BOL} = \varepsilon_{BOL} I_D \cos(\theta) P_0 = 147.82 \text{ W/m}^2 \quad (34)$$

As can be seen in Equation (34), the other values that need to be defined are the inclination angle  $\theta$  and the inherent degradation  $I_D$ . The first one depends on the mission characteristics: as the SOHO nominal condition is to point always to the Sun, the value could be assumed to be 0 deg; however, this would mean that a really strict requirement is imposed to the ADCS subsystem. To avoid that, a  $\theta = 30$  deg pointing budget is considered, allowing the S/C to rotate without the risk of losing its power generation ability. The inherent degradation  $I_D$  is

instead defined to take into account the loss due to cells and lines connections with each other and various external factors; its value is assumed to be 0.92, given the higher requirements in the production phase of the solar arrays<sup>[62]</sup>. An important parameter to correctly size the solar arrays is the *End of Life* (EOL) specific power  $P_{EOL}$ , which can be computed given the lifetime degradation of the cells  $L_{life}$ . This one is computed from the degradation per year, estimated to be  $dpy = 1.8\%/year$ <sup>[16]</sup>.

$$\begin{cases} L_{life} = (1 - dpy)^{lifetime} = 0.9556 \\ P_{EOL} = L_{life} \cdot P_{BOL} = 141.26 \text{ Wh} \end{cases} \quad (35)$$

$$A_{SA} = \frac{P_{SA}}{P_{EOL}} = 15.92 \text{ m}^2 \quad (36)$$

The total area covered by the solar cells can be obtained via Equation (36). The resulting value of  $15.92 \text{ m}^2$  must be expressed as an integer multiple of the cell area, which is  $0.0024 \text{ m}^2$ <sup>[62]</sup>, so a minimum of 6605 cells is required. However, to compute the real number of cells, it is necessary to know how many of them have to be in series. This is obtained considering the voltage of the system, which must be 28 V, and dividing it by the voltage of each cell, equal to 0.404 V<sup>[62]</sup>; this results in 70 cell connected together in series. This is a little less than the one actually mounted on the S/C: 77 in series for 3 of the 4 double string of each section; the last string has 78 cells instead<sup>[62]</sup>. This discrepancies between calculated and real data is to be expected: as the calculation done during the design phase of the mission used preliminary data regarding the cells, a lower voltage per cell could have been considered. Moreover, a safety margin can be taken into account for cell failure during the mission. As can be seen, the difference is approximately 10%, which is compliant with the general values used for margins.

Finally, the real voltage produced can be obtained by multiplying the number of cell in series with the expected voltage of each one, obtaining a value of  $V_{real} = 28.28 \text{ V}$ , slightly higher than the desired one, but enough to allow some losses in the power transmission system without losing performance.

From this calculations, a total of 6650 cells need to be mounted on the solar array surface, for a total area of  $A_{SA} = 16.03 \text{ m}^2$  occupied. This is higher than the real values that can be observed on the S/C: in fact, SOHO mounts a total of 4944 cells divided in 8 section, two on each one of the four panels, for a total area of  $11.92 \text{ m}^2$ .

The difference can be explained by analyzing a few factors:

- The EOL power computed by our calculations is much higher than the required one of 1400 W<sup>[62][16]</sup>. This is probably due to different margins and assumptions used during sizing. This can also be explained by considering that the sizing done during the design phase probably started by imposing the final EOL power to be a little higher than 1400 W. The workflow done by us starts by imposing a BOL margined power, where the EOL condition is obtained through the use of degradation factors, which can be hard to estimate a priori.
- Some of the data gathered for our calculations are obtained from the final product. This data however are most likely to differ (even slightly) from the one used during the satellite development: as said before, some assumptions made during the S/C design were not respected in the completed product. This implies that some of the choices had to be more or less conservative than what was later found as necessary.
- The lifetime considered for the solar panel during design phase could be different. This changes the total degradation over time, thus altering the computation of power losses.

Finally, the mass of the solar arrays  $m_{SA}$  can be computed knowing the density  $\rho$  and thickness  $th$  of the cells; SOHO's solar cells are made of Silicon ( $\rho_{Si} = 2330 \text{ kg/m}^3$ ,  $th_{Si} = 210 \mu\text{m}$ ) and CMX glass ( $\rho_{gl} = 2600 \text{ kg/m}^3$ ,  $th_{gl} = 100 \mu\text{m}$ )<sup>[16,62,67]</sup>:

$$m_{SA} = A_{SA}(\rho_{Si} h_{Si} + \rho_{gl} h_{gl}) = 12.02 \text{ kg} \quad (37)$$

The resulting value does not take into account the mass of the structure sustaining the solar arrays nor the pointing mechanisms, so it has to be intended as the total mass of the solar cells, while the real mass of the complete solar arrays system will be higher.

### 6.3.2 Batteries

As said before, the mission objective is to always point to the Sun, so the solar arrays are the main power source during all the nominal mission. The batteries are necessary to ensure that the S/C survives two critical conditions: *Initial Sun Acquisition* (ISA) and off-nominal situations. The first one nominally happens once the satellite detaches from Centaur and needs to have sufficient power to guarantee that the actuators have time to point the solar arrays towards the Sun, and also to perform the Sun-pointing after the end of the Emergency (ESR) mode. For the off-nominal conditions, the batteries shall have sufficient power to guarantee the survival of the S/C until the next available downlink period in order to send to the ground station the last data to alert of its unexpected conditions and receive instructions from the ground control.

To size the batteries, the minimum power required by the S/C has to be known. Since the batteries are used in off-nominal conditions, it can be safely assumed that all the payloads are turned off in order to reduce the power consumption. Moreover, it can be assumed that the High Gain Antenna isn't powered as the emergency communications are done using the Low Gain ones. Thus, the power requirement is  $P_{req} = 560 \text{ W}$  (from Section 6.2). The maximum time window between two communication periods computed in the TTMTTC analysis is  $3.73 \text{ hrs}$ , which can be approximated to  $T_{req} = 4 \text{ hrs}$  to allow extra time for correct downlink and potential final uplink commands.

The combination chosen for the batteries is Nickel-Cadmium. This is the most common type of secondary battery, due to their low cost (due to their popularity in mass production) and good rechargeability. Firstly, the required capacity can be computed from Equation (38), where  $N = 2$  is the number of batteries<sup>[16]</sup>, *DoD* is the *Depth-of-Discharge* of the batteries assumed to be 0.7 given the expected low amount of cycles that the batteries have to go through, and  $\eta_{line}$  is the line efficiency, assumed to be 0.8 as done for the solar arrays:

$$C = \frac{P_{req} T_{req}}{DoD N \eta_{line}} = 4000 \text{ Wh} \quad (38)$$

The electric charge of the batteries can then be computed dividing the capacity by the system voltage of  $28 \text{ V}$ , resulting in  $142.9 \text{ Ah}$ .

To better refine the sizing, the number of cell per series must be computed from the voltage of the single cell, equal to  $V_{cell} = 1.35 \text{ V}$ : a total of 21 cell must be placed in series to reach the required  $V_{sys} = 28 \text{ V}$  (with a little overshoot of  $0.35 \text{ V}$ ).

Therefore, the capacity of a single string can be computed via Equation (39), where  $\mu$  is the package efficiency, assumed to be the standard value of 0.8, and  $C_{cell} = 20 \text{ Ah}$ :

$$C_{string} = \mu C_{cell} V_{sys} = 453.6 \text{ Wh} \quad (39)$$

To get the wanted capacity, a total of 9 strings must be put in parallel.

The actual system capacity is then  $C_{real} = 4082.4 \text{ Wh}$ . It is not possible to judge how close this value is to the real data due to the lack of essential information.

Finally, the batteries' mass and volume can be computed knowing the specific energy  $E_m = 40 \text{ Wh/kg}$  and energy density  $E_V = 90 \text{ Wh/dm}^3$  of the Ni-Cd type, thus obtaining a total mass of  $m_{batt} = 102.06 \text{ kg}$  and a volume of  $V_{batt} = 45.36 \text{ dm}^3$ .

The results obtained tend to overestimate the the actual SOHO S/C configuration, mostly due to the use of high margins and different design philosophies.

## 7 Space Segment & OBDH

### 7.1 Space Segment

The spacecraft is divided in two main modules: the *Payload Module* (PLM) and the *Service Module* (SVM) that are connected through an interface ring.

The SVM is structured as a box, with aluminum honeycomb panels connected to a corrugated aluminum cylinder by four shear webs. The lateral panels house various subsystems, including data-handling, communication, attitude and orbit control, and power. The upper part of the box contains the propulsion subsystem, tank, and thruster masts, whereas the high-gain antenna is integrated into the aft section of the central cylinder<sup>[36]</sup>.



Figure 15: SOHO launch configuration<sup>[5]</sup>

The PLM is equipped with an optical bench for conducting experiments and is made up of four upper lateral panels and a top panel connected to a central cylinder through shear webs. The lower section, which comprises three lower lateral panels connected to the central cylindrical tube via shear webs and floors, is where the PLM electronics are housed.

The S/C is connected to the launcher (an ATLAS II-AS) through the *Large Payload Fairing* (LPF)<sup>[26]</sup>. This connection is kept until the end of the LEOP phase as the Centaur upper stage detaches only once the TTP starts<sup>[8]</sup>. No official data can be found on how the S/C was placed inside the fairing, but it is possible to analyse the folded configuration shown in Figure 15: the solar arrays are closed and attached to the SVM and the *High-Gain Antenna* (HGA) is retracted inside its base. This is the same configuration used to place the S/C inside the launcher as no other interfaces are visible nor possible due to the limitations imposed by the components and their configuration. In this case, the fairing ring is connected to the lower base of the SVM (as can be also seen in this image<sup>[24]</sup>), probably with the HGA enclosed in the interface piece. After the launch phase and after the separation from the Centaur, both solar arrays and HGA can be fully deployed.

#### 7.1.1 Configuration

Understanding the configuration and reverse sizing of the space segment, an overview of all the subsystems is presented to better analyze all the components of the S/C.

**Payload module** Table 29 presents the main characteristics of the payloads regarding weights and dimensions. Some information are not publicly available as can be seen by the blank spots.

Payload	Weight [kg]	Dimensions	Payload	Weight [kg]	Dimensions
GOLF	37.8	—	VIRGO <sup>[68]</sup>	14.4	300 x 90 x 90 [mm]
ERNE	—	—	COSTEP	21.2	—
CELIAS <sup>[69]</sup>	29.6	—	SWAN	13.2	—
LASCO <sup>[52]</sup>	67.6	135 x 34 x 32 [cm]	UVCS	117.3	—
EIT	14	—	CDS <sup>[70]</sup>	95	1.7 x 0.50 x 0.46 [m]
SUMER	95.9	—	MDI	37.8	—

Table 29: Payloads information<sup>[17]</sup>

These instruments are mounted on the PLM as can be seen in Figure 15 and they are arranged to better conduct experiments since their view with the Sun cannot be obstructed.

**Propulsion subsystem** The S/C mounts a total of 16 hydrazine monopropellant thrusters: the *MRE-1.0* by *Northrop Grumman Corporation*, with a weight of  $0.5\text{ kg}$  each<sup>[18]</sup>. Each thruster has a width of  $190\text{ mm}$  and a length of  $38\text{ mm}$ , for a volume of  $2.1548 * 10^{-4}\text{ m}^3$  each and a total one of  $0.0034\text{ m}^3$ . The thrusters are organized in 8 *Dual Thruster Modules* (DTM), located in three different parts of the S/C: two are located directly on the upper platform, two are on the bottom side and the other four (5 to 8) are placed on masts that extend from the upper platform of the service module. This configuration guarantees that both long burn manoeuvres (mostly done during the transfer phase) and attitude correction manoeuvres. The pairs 1 and 2 are inclined by  $30\text{ deg}$ <sup>[11]</sup> upwards, to limit plume impingement effect on the payloads.

The tank mounted on the satellite is the *80263-1 propellant tank* by *Northrop Grumman Corporation*<sup>[34]</sup>. It is mounted in the central cylinder and occupies a volume of  $0.4612\text{ m}^3$ . This placement guarantees minimal impact of the fuel variation of the S/C inertias: during the mission, as the fuel is consumed (starting with  $251\text{ kg}$  of hydrazine), the weight distribution changes; to avoid the S/C inertias change too drastically (thus interfering with the ADCS subsystem and requiring constant updates to the control law), the position of the tank is critical.

**TTMTC subsystem** The *High Gain Antenna* HGA is a  $804\text{ mm}$  reflector antenna having a gain of  $22.7\text{ dBi}$ . It is made of a carbon fiber reflector, an aluminum feed cone (with a crossed dipole feed) and a reflective disk on top. During launch, the HGA is rigidly attached to the spacecraft and is released only after spacecraft separation. In fact, the HGA has 2 degrees of freedom in order to always point towards Earth during its nominal operations<sup>[71]</sup>. The antenna is positioned on the bottom part of the spacecraft, where it is always kept in complete shade (during nominal operations) by the solar array wings and by the body: this allows to reduce the cooling requirement on the device, which better works with lower temperatures and would be damaged if exposed for too long to direct solar radiation.

Two *Low Gain Antennas* (LGA), used only for low telemetry or emergency transmissions, are quadrifilar helix antennas mounted on  $+Z$  and  $-Z$  side of the spacecraft. This way they ensure omni-directional coverage. Considering the reference frame of the antennas, the antenna pattern displays quasi-rotationally symmetric and quasi-isotropic characteristics in the elevation region spanning from 0 to  $108.5^\circ$ . From an analysis of the CAD model<sup>[6]</sup> of the spacecraft, it is possible to deduce that each antenna is approximately  $319\text{ mm}$  long with a diameter of  $31\text{ mm}$ .

**ADCS subsystem** Regarding the attitude control system, together with the thrusters, the S/C mounts four reaction wheels, with diameter of  $365\text{ mm}$  and height of  $125\text{ mm}$  each<sup>[72]</sup>. They weight  $6.70\text{ kg}$  each. This data does not account for the necessary electronics: each *Wheel Drive Electronic* (WDE) weights  $4.67\text{ kg}$  and occupies a volume of  $258mm \times 181mm \times 143mm$ <sup>[72]</sup>. The wheels are positioned in a pyramid configuration: this is the most compact configuration that still achieves full redundancy (the S/C can still be completely controlled even if one wheel fails).

The sensors mounted include two star tracker, which weight  $7.2\text{ kg}$  each<sup>[47]</sup> and two fine pointing sun sensors whose weight is  $2.03\text{ kg}$  each (including the electronics), occupying a dimension of  $15cm \times 10cm \times 7cm$  for each sensor and  $20cm \times 13cm \times 6cm$  for each associated electronics. The star trackers are positioned along the  $+Z$  direction to protect them from direct sun exposure that would damage it. The Fine Pointing Sun Sensors are placed along the  $+X$  direction as they have to be constantly face the sun during nominal operations. The *Sun Acquisition Sensors* (SAS) are instead placed both along the  $+X$  direction and on the  $\pm Z$  direction. This way they guarantee easier detection of the sun position during the initial alignment phase and they also act as trigger for the sun protection of the star trackers in non-nominal conditions: if a SAS detects the presence of the Sun, its associated Star tracker gets covered to avoid damaging it.

**Thermal subsystem** The thermal subsystem is different with respect to the other parts of SOHO: its importance relies on the passive and active components that are vital to keep the whole S/C under the working temperatures. For this reason a *Multi-layer Insulation* MLI blanket covers almost all the spacecraft, leaving unprotected all the active systems such as antennas, thrusters and payloads sensors. Its volume is considered to be negligible for the scope of this discussion since does not interfere with other systems and its positioning is related to the last steps of the configuration. The internal surfaces of the S/C are covered in black paint to guarantee good and predictable radiative coupling and to minimize temperature gradients. This layer is thin, thus its volume and weight can be considered negligible.

The final configuration, as it was shown in the sizing, requires a mixed solution with both heaters and radiators. The radiators have an area of  $6.52 \text{ m}^2$ , a thickness of 23 mm and a weight of 78.3 kg. The heaters are considered to be negligible since their volume and weights are small when compared with other parts. The final surface left is occupied by the MLI (81.4 kg).

**Power subsystem** Solar arrays are deployed in a fixed configuration composed of two wings in the +Y and -Y direction<sup>[61]</sup>, each consisting of 2 solar panels and 1 yoke panel; the total dimensions of each wing are  $3.657\text{m} \times 2.300\text{m}$  with a thickness of the solar cell of  $210\mu\text{m}$  and a thickness of the CMX glass layer of  $100\mu\text{m}$ <sup>[16,62,67]</sup>: this adds up to a total weight of 12.02 kg (w/o honeycomb). Their position is strictly related to the most sun viewing face: for this reason they are facing the Sun in the +X direction; furthermore, they have to be placed on the lowest part of spacecraft as they would otherwise obstruct the view of the payloads. The positioning of this element plays a crucial role in determining the weight distribution of the spacecraft. While the center of mass can be assumed to be at the center of the spacecraft, thanks to the payloads' weight compensating for the wings, the inertias along the Y and Z axes are significantly impacted. Nonetheless, this should not cause major issues, given that the spacecraft's main spin axis is aligned with the X axis, and the wings exhibit symmetry with respect to it. The batteries are instead collocated inside the main S/C body with a total volume of  $6 \text{ dm}^3$  and a weight of 14 kg. Their positioning would mostly be dictated by the inertia of the S/C, allowing for a small tune of it.

### 7.1.2 CAD representation

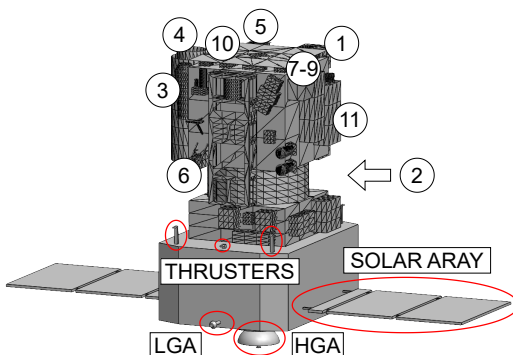


Figure 16: CAD<sup>[6,7]</sup> of the SOHO S/C

- |          |           |
|----------|-----------|
| 1. SUMER | 7. CELIAS |
| 2. CDS   | 8. COSTEP |
| 3. EIT   | 8. ERNE   |
| 4. UVCS  | 9. GOLF   |
| 5. LASCO | 10. VIRGO |
| 6. SWAN  | 11. SOI   |

Table 30: Payloads enumeration<sup>[20,21]</sup>

As can be seen in the CAD modeled using SOLIDWORKS<sup>[7]</sup>, all the sized components can be reconstructed to visually represent the entire S/C. Some components are hidden inside or behind the SOHO body. This proves that all the dimensions fit inside the model thus validating the results obtained. The total dimensions of the S/C are  $4.3 \times 2.7 \times 3.65$  meters as previously discussed and the weight is respected.

## 7.2 OBDH

### 7.2.1 Architecture

**Overview** The *On Board Data Handling* (OBDH) subsystem manages the storage and processing of information coming from all the subsystems of the S/C, including the scientific data produced by the payload equipment. The architecture is centralized and it is summarized by Figure 17<sup>[8]</sup>:

**Management** The heart of this subsystem is composed by the *Central Data Management Unit* (CDMU), which is composed by a redundant intelligent processing unit including a 16 bit MAS281 microprocessor. It is responsible for<sup>[13,44]</sup>:

- Onboard processing.
- Inter-instrument data exchange.
- Thermal control of SVM and PLM.
- Acquisition and management of the data coming from experiments and SVM.
- Organization and transmission of the data to the ground stations.
- Decoding, validation and distribution of the commands coming from ground to the payload module and to the SVM.
- Data storage during periods of lack of visibility with the ground.
- Maintenance and distribution of time base references for synchronization and time tag purposes.
- On board surveillance and monitoring to ensure the safety of the S/C

It is fundamental for the processor to be redundant, since it is the only node of the subsystem: a failure of it would mean the loss of all the functions above illustrated, and therefore the irreversible ending of the mission. The choice of the centralized architecture was likely made because the CDMU is considered quite robust, so a single failure would affect just one line.

**Bus** Data exchanges between the computers and the different subsystems are provided by the use of the digital OBDH bus, which is controlled by the central processor. The transmission of information occurs by using separate lines for interrogation, in which the computer gives commands or requests, and for response, to transmit data and updates to the computer. The bit rate used for both the transmissions is 524 kHz<sup>[13]</sup>, using as format a Litton based code.

**Memory** The storage relies on one tape recorder of 1 Gigabit plus one fully self-redundant solid state recorder of 2 Gigabits capacity<sup>[13]</sup>. Part of the memory is dedicated to future system upgrades, as seen in Table 31 the PROM set aside differs for data handling and attitude control unit. In addition to the computer ROM, dedicated RAM is available for data handling and for AOCS, with the values showed in Table 31.

Automatic failure detection and reconfiguration is provided and vital spacecraft parameters are retained in a special “context memory”<sup>[44]</sup>.

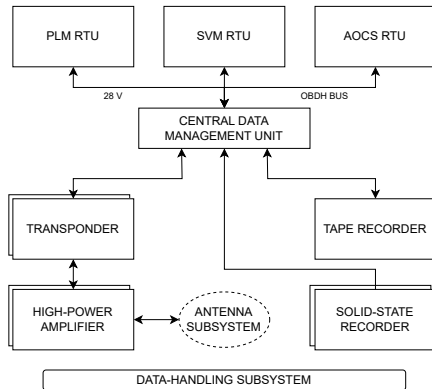


Figure 17: OBDH architecture<sup>[8]</sup>. Duplicated rectangles indicate duplicated hardware

	Data Handling	Attitude Control
Memory size-RAM	64 kwords	64 kwords
Memory size-PROM	40 kwords	32 kwords
Margin-RAM	22 %	60 %
Margin-PROM	12 %	41 %
Context memory-RAM	8 kbyte	

Table 31: dedicated memory<sup>[14]</sup>

In addition to the previous RAM, another one is dedicated to preserve temporary data in case of unwanted interruptions and malfunctions in the system. Further margins were applied to the memory size to make sure not to saturate the allocated memory during operations.

The data are further contextualized and verified at the end of Section 7.2.2.

**Computational units** Three *Remote Terminal Units* (RTU) are used to simplify the data interfaces, as well as telemetry and command functions. These RTUs are respectively dedicated to PLM (*Payload Module*), SVM (*Service Module*) and ACU (*Attitude Control Unit*). The ACU is based on the same microprocessor used for CDMU. To avoid critical malfunctions the system is fully redundant, furthermore in case of failures, an independent mode (hardwired) provides a safe mode to protect the system.

**Time** Universal time (UTC) is generated on board by an *Ultra Stable Oscillator* (USO) and distributed to the experiments<sup>[44]</sup>. The USO drives a clock that is maintained within  $\pm 20$  ms<sup>[13]</sup>.

**Data protocol** Data exchange is controlled periodically by a COBS software, running on the OBDH. Two 16 bit words are sampled every 16 seconds from the Master. The words are formed as follow: a validity bit, bit 2-5 are destination address, bits 6-10 are the command identifier and bits 11-15 correspond to the block length. The inter-instrument communication process can be divided in two states: active or disabled; in the second one, all instruments are set to the stand-by.

Bit rates [bit/s]	1.19 - 54.6 - 214.25
Command rate [kbit/s]	2
Clock stability	$\pm 6 \times 10^{-9}$
Acquisition channel	992
Command channel	660

Table 32: Data handling specifications<sup>[14]</sup>

As seen in Table 32, the bit rate for the command is maintained constant while the one dedicated to the data handling is variable, depending on the usage of the payload's instruments.

### 7.2.2 OBDH Sizing

The sizing is conducted with an *estimation by similarity* process. The total values are computed via Equation (41), which is reported only for the total throughput case (i.e. total KIPS, thousands of instructions per second), but that is valid for total code [words] and total data [words] too:

$$KIPS_{fun} = KIPS_{typ} \frac{f_{acq}}{f_{typ}} \quad (40) \quad KIPS_{tot} = \sum_{i=1}^{n_{fun}} k_{fun,i} KIPS_{fun,i} \quad (41)$$

Where  $k_{fun}$  includes the number of components that execute a specific function (listed in the following tables). In the tables below all the functions allocated to the computer, divided by subsystem, are listed:

PS							
Components	Number	Code [words]	Data [words]	Typical KIPS	Typical Frequency [Hz]	Acquisition Frequency [Hz]	KIPS
Tank	1	—	—	—	—	—	—
Tank control valve	2	800	1500	3	0.1	0.1	3
Latch valves	2	800	1500	3	0.1	0.1	3
Fuel control valve	8	800	1500	3	0.1	0.1	3
Tank pressure sensor	1	800	1500	3	0.1	0.1	3
Branch pressure sensor	2	800	1500	3	0.1	0.1	3
<b>Total</b>		12000	22500				45
Margined (+400%)		60000	112500				225

TTMTC							
Components	Number	Code [words]	Data [words]	Typical KIPS	Typical Frequency [Hz]	Acquisition Frequency [Hz]	KIPS
S-band HGA	1	—	—	—	—	—	—
S-band LGA	2	—	—	—	—	—	—
Command processing	1	1000	4000	7	10	10	7
Telemetry processing	1	1000	2500	3	10	10	3
<b>Total</b>		2000	6500				10
Margined (+400%)		10000	32500				50

AOCS							
Components	Number	Code [words]	Data [words]	Typical KIPS	Typical Frequency [Hz]	Acquisition Frequency [Hz]	KIPS
Reaction wheels control	4	1000	300	5	2	$10^{[72]}$	25
Thruster control	16	600	400	1.2	2	1	0.6
Star tracker	2	2000	15000	2	0.01	1	200
Rate integrating gyro	3	800	500	9	10	10	9
Fine pointing Sun sensor	2	500	100	1	1	1	1
Sun acquisition sensor	3	500	100	1	1	1	1
Kinematic integration	1	2000	200	15	10	10	15
Error determination	1	1000	100	12	10	10	12
Attitude determination	1	15000	3500	150	10	10	150
Attitude control	1	24000	4200	60	10	10	60
Complex ephemeris	1	3500	2500	4	0,5	1	8
Orbit Propagation	1	13000	4000	20	1	1	20
<b>Total</b>		81000	54100				806.6
Margined (+400%)		405000	270500				4033

TCS							
Components	Number	Code [words]	Data [words]	Typical KIPS	Typical Frequency [Hz]	Acquisition Frequency [Hz]	KIPS
Thermal control	2	800	1500	3	0.1	0.1	3
<b>Total</b>		1600	3000				6
Margined (+400%)		8000	15000				30

EPS							
Components	Number	Code [words]	Data [words]	Typical KIPS	Typical Frequency [Hz]	Acquisition Frequency [Hz]	KIPS
Solar panels	2	—	—	—	—	—	—
Batteries	2	—	—	—	—	—	—
Cables & Harness	1	—	—	—	—	—	—
Power voltage control	1	1200	500	5	1	0.1	0,5
Power current control	1	1200	500	5	1	0.1	0,5
<b>Total</b>		2400	1000				1
Margined (+400%)		12000	5000				5

OS							
Components	Number	Code [words]	Data [words]	Typical KIPS	Typical Frequency [Hz]	Acquisition Frequency [Hz]	KIPS
I/O Device handlers	1	2000	700	50	5	1	10
Test & Diagnostic	1	700	400	0.5	0.1	1	5
Math utilities	1	1200	200	0.5	0.1	1	5
Executive	1	3500	2000	60	10	10	60
Runtime kernel	1	8000	4000	60	10	10	60
Complex autonomy	1	15000	10000	20	10	10	20
Fault detection (monitors)	1	4000	1000	15	5	1	3
Fault correction	1	2000	10000	5	5	10	10
<b>Total</b>		36400	28300			173	
Margined (+400%)		182000	141500			865	

An analysis of the possible operating situations can be performed to evaluate the worst case scenario for the OBDH subsystem. Station keeping (SK), executed with thrusters, has been identified as the most demanding operation for the OBDH. During SK, the payloads are de-activated to avoid contamination from the thrusters' plume impingement. ROM, RAM and Throughput are computed via Equations (42) to (44) and results are shown in Table 33:

$$ROM_{code} = \frac{code_{tot} [\text{words}] 16 [\frac{\text{bit}}{\text{word}}]}{8 [\frac{\text{bit}}{\text{byte}}] 1000 [\frac{\text{byte}}{\text{kbyte}}]} [\text{kB}] \quad ROM_{data} = \frac{data_{tot} [\text{words}] 16 [\frac{\text{bit}}{\text{word}}]}{8 [\frac{\text{bit}}{\text{byte}}] 1000 [\frac{\text{byte}}{\text{kbyte}}]} [\text{kB}] \quad (42)$$

$$RAM = \frac{(code_{tot} [\text{words}] + data_{tot} [\text{words}]) 16 [\frac{\text{bit}}{\text{word}}]}{8 [\frac{\text{bit}}{\text{byte}}] 1000 [\frac{\text{byte}}{\text{kbyte}}]} [\text{kB}] \quad (43) \quad TP = \frac{TP_{tot} [\text{KIPS}]}{1000 [\frac{\text{KIPS}}{\text{MIPS}}]} [\text{MIPS}] \quad (44)$$

STATION KEEPING	AOCS	PS	TTMTC	TCS	EPS	OS	Payload	Total
Throughput [MIPS]	806.6	45	10	6	1	173	0	1041.6
Margined [MIPS]	4033	225	50	30	5	865	0	5208
Code [words]	81000	12000	2000	1600	2400	36400	0	135400
Margined [words]	405000	60000	10000	8000	12000	182000	0	677000
Data [words]	54100	22500	6500	3000	1000	28300	0	115400
Margined [words]	270500	112500	32500	15000	5000	141500	0	577000

Table 33: OBDH worst case scenario: station keeping

SK	Tot Code (ROM) [kB]	Tot Data [kB]	RAM [MB]	TP [MIPS]
Total	270.8	230.8	0.5016	1.0416
Margined	1354	1154	2.508	5.208

Table 34: Station keeping

NM	Tot Code (ROM) [kB]	Tot Data [kB]	RAM [MB]	TP [MIPS]
Total	246.8	185.8	0.4326	0.9966
Margined	1234	929	2.163	4.983

Table 35: Nominal mode

In Table 34 and Table 35 results are shown. Normal mode differs from SK in the de-activation of the propulsion subsystem, since the nominal attitude control is handled by the reaction wheels (i.e. PS column is set to 0). However, in NM the scientific payloads are active and their data ( $20\text{ MB/day}^{[13]}$ ) is recorded by the OBDH; the RAM will be influenced by the amount of code and data of the scientific measurements to be processed and this shall be taken into account for a refined design of the OBDH subsystem (since no values have been found on payloads' code, data and TP, this consideration is only qualitative and not numerically supported). The obtained necessary ROM and RAM size (total values, not margined) are in line with the values described in the Table 31 (in Section 7.2.1), thus validating the model. The obtained values are different from the real ones because the presented sizing has been conducted with an *estimation by similarity* process; more refined values could be obtained with more precise knowledge of the specifics of the components mounted on the spacecraft.

## 8 References

- [1] “SOHO Image Gallery,” ESA / NASA. [Online]. Available: <https://soho.nascom.nasa.gov/gallery/Spacecraft/>
- [2] B. Lehmann, A. J. Schnorjk, and S. Jallade, “The SOHO thrusters temperature control,” in *Sixth European Symposium on Space Environmental Control Systems*, ser. ESA Special Publication, T. D. Guyenne, Ed., vol. 400, Aug. 1997, p. 133. [Online]. Available: <https://ui.adsabs.harvard.edu/abs/1997ESASP.400..133L/abstract>
- [3] Domingo, Fleck, Poland, “SOHO - Science Operations Plan,” [https://www.nasa.gov/wp-content/uploads/2015/04/156579main\\_sop-soho.pdf](https://www.nasa.gov/wp-content/uploads/2015/04/156579main_sop-soho.pdf), 1995, eSA S/95/088/972.
- [4] P. Poinas, J. Cande, “Soho spacecraft thermal control aspects,” *Sixth European Symposium on Space Environmental Control Systems, held in Noordwijk, The Netherlands, 20-22 May, 1997. Compiled by T.-D. Guyenne. European Space*, 1997.
- [5] “Soho ready for launch,” ESA. [Online]. Available: [https://www.esa.int/ESA\\_Multimedia/Images/1998/01/Soho\\_ready\\_for\\_launch](https://www.esa.int/ESA_Multimedia/Images/1998/01/Soho_ready_for_launch)
- [6] Chris Meaney. NASA, “Solar and Heliospheric Observatory (partial LWO file).” [Online]. Available: <https://nasa3d.arc.nasa.gov/detail/soho>
- [7] “SOLIDWORKS,” Dassault Systèmes - SolidWorks Corporation. [Online]. Available: <https://www.solidworks.com>
- [8] F. C. Vandenbussche, “Soho - the trip to the l1 halo orbit,” <https://www.esa.int/esapub/bulletin/bullet88/vande88.htm>, 1996.
- [9] D.W. Dunham, S. J. Jen, C.E. Roberts, A.W. Seacord II, P.J. Sharer, D.C. Folta, D.P. Muñonen, “Transfer trajectory design for the SOHO libration-point mission,” *IAC 1992 Congress Proceedings, 43rd International Astronautical Congress*, 1992. [Online]. Available: <https://dl.iafastro.directory/event/IAC-1992/paper/IAF-92-0066/>
- [10] R. D. Headrick and J. N. Rowe, “Solar and Heliospheric Observatory (SOHO) Flight Dynamics Simulations Using MATLAB,” 1996. [Online]. Available: <https://ntrs.nasa.gov/api/citations/19960035757/downloads/19960035757.pdf>
- [11] R. Short, J. Behuncik, “The solar and heliospheric observatory (soho) mission: An overview of flight dynamics support of the early mission phase,” 1996. [Online]. Available: <https://ntrs.nasa.gov/api/citations/19960035770/downloads/19960035770.pdf>
- [12] David W. Dunham and Craig E. Roberts, “Stationkeeping techniques for libration-point satellites,” *The Journal of the Astronautical Sciences*, Vol. 49, No.1, January-March 2001, pp. 127-144, 2001. [Online]. Available: <https://link.springer.com/article/10.1007/BF03546340>
- [13] Domingo, Fleck, Poland, “The SOHO mission: An overview,” *Solar Physics*, no. 162, pp. 1–37, 1995.
- [14] F. Vandenbussche, “The soho spacecraft,” <https://www.esa.int/esapub/bulletin/bullet84/vdbus84.htm>, 1995.
- [15] “SOHO Instrument Resources.” [Online]. Available: <https://soho.nascom.nasa.gov/data/archive/instruments.html>

- [16] P. Rumler, H. Schweitzer, "Soho power system performance during 6 years in orbit," *Space Power, Proceedings of the Sixth European Conference held 6-10 May, 2002 in Porto, Portugal. Edited by A. Wilson. European Space Agency, ESA SP-502, 2002.*, p.141, 2002.
- [17] Huber, Martin C E., "The SOHO Concept and Its Realisation," *Space Science Reviews*, 1992.
- [18] "MRE-1.0 Monopropellant Thruster," [https://wpcontent.ot5o9s93syrb.net/wp-content/uploads/MRE-10\\_MonoProp\\_Thruster.pdf](https://wpcontent.ot5o9s93syrb.net/wp-content/uploads/MRE-10_MonoProp_Thruster.pdf), Northrop Grumman Corporation.
- [19] Olive, Jean-Philippe ; Chaloupy, Marc ; Schweitzer, Helmut, "The soho spacecraft: a solar cycle mission," *SOLMAG 2002. Proceedings of the Magnetic Coupling of the Solar Atmosphere Euroconference and IAU Colloquium 188, 11 - 15 June 2002, Santorini, Greece. Ed. H. Sawaya-Lacoste. ESA SP-505. Noordwijk, Netherlands: ESA Publications Division, ISBN 92-9092-815-8, 2002, p. 41 - 44*, 2002.
- [20] "Schematics of the SOHO spacecraft, showing the locations of the twelve experiments," ESA. [Online]. Available: <https://www.esa.int/esapub/bulletin/bullet84/images/domi843.gif>
- [21] "SOHO Spacecraft Model," NASA, 2017. [Online]. Available: <https://science.nasa.gov/resource/soho-spacecraft-model/>
- [22] W. Worrall, D. Muñonen & R. Menrad, "The soho ground segment and operations," <https://www.esa.int/esapub/bulletin/bullet84/worral84.htm>, 1995.
- [23] Alessi, Tommei, Holbrough, Beck, "ON THE REENTRY DESIGN FOR THE SOHO MISSION," in *7th European Conference on Space Debris*, Flohrer, Schmitz, Ed. ESA Space Debris Office, 2017.
- [24] Berner, Domingo, "The SOHO Payload and Its Testing," <https://www.esa.int/esapub/bulletin/bullet84/domi84.htm>, 1995.
- [25] "JPL NASA Horizons Web Application," Jet Propulsion Laboratory, 2023. [Online]. Available: <https://ssd.jpl.nasa.gov/horizons/app.html#/>
- [26] "Atlas Launch System Mission Planner's Guide," Lockheed Martin, 2001.
- [27] "SOHO's Launch," ESA / NASA. [Online]. Available: [https://soho.nascom.nasa.gov/about/launch\\_vehicle.html](https://soho.nascom.nasa.gov/about/launch_vehicle.html)
- [28] C. Roberts, "The soho mission 11 halo orbit recovery from the attitude control anomalies of 1998," 05 2003.
- [29] "Propulsion Products Catalog," Northrop Grumman. [Online]. Available: <https://cdn.prd.ngc.agencyq.site/-/media/wp-content/uploads/NG-Propulsion-Products-Catalog.pdf>
- [30] "SOHO-Spacecraft-Events," ESA / NASA. [Online]. Available: [https://soho.nascom.nasa.gov/soc/soho\\_events/SOHO-Spacecraft-Events.pdf](https://soho.nascom.nasa.gov/soc/soho_events/SOHO-Spacecraft-Events.pdf)
- [31] David Dunham Craig Roberts, "The solar and heliospheric observatory, the longest halo-orbiting mission," *IAC 2021 Congress Proceedings, 72nd International Astronautical Congress (IAC), Dubai, United Arab Emirates, 2021*. [Online]. Available: <https://dl.iafastro.directory/event/IAC-2021/paper/66035/>

- [32] Craig E. Roberts, "The SOHO Mission L1 Halo Orbit Recovery From the Attitude Control Anomalies of 1998," in *Libration Point Orbits and Applications Conference*, Parador d'Aiguablava, Girona, Spain, 05 2003.
- [33] "Concurrent Design Facility Studies Standard Margin Philosophy Description," ESA.
- [34] "Diaphragm Tanks Data Sheets," <https://www.northropgrumman.com/space/diaphragm-tanks-data-sheets-sorted-by-volume>, Northrop Grumman Corporation.
- [35] "Titanium Ti-6Al-4V (Grade 5), Annealed," <https://asm.matweb.com/search/SpecificMaterial.asp?bassnum=MTP641>, MatWeb LLC.
- [36] "Soho (solar and heliospheric observatory)," <https://www.eoportal.org/satellite-missions/soho>, 2012.
- [37] "Spacecraft emergencies and pointing modes: An overview," <https://soho.nascom.nasa.gov/soc/esr/>, NASA.
- [38] NASA, "General mission analysis tool (gmat)." [Online]. Available: <https://software.nasa.gov/software/GSC-17177-1>
- [39] G. S. Tech, "Atmospheric attenuation," [https://propagation.ece.gatech.edu/ECE6390/project/Fall2012/Team09/Team9GeoSatTech\\_website\\_FINAL/SatCom%20website/atmosphericAttenuation.html](https://propagation.ece.gatech.edu/ECE6390/project/Fall2012/Team09/Team9GeoSatTech_website_FINAL/SatCom%20website/atmosphericAttenuation.html).
- [40] "26-m antenna subnet telecommunications interfaces," <https://deepspace.jpl.nasa.gov/dsndocs/810-005/102/102.pdf>, NASA.
- [41] C. C. for Space Data Systems, "PROCEEDINGS OF THE CCSDS RF AND MODULATION SUBPANEL 1E MEETING OF MAY 2001 CONCERNING BANDWIDTH-EFFICIENT MODULATION," = <https://public.ccsds.org/Pubs/B20x0y2.pdf>, 2001.
- [42] "26-m Antenna Subnet Telecommunications Interfaces." [Online]. Available: <https://deepspace.jpl.nasa.gov/dsndocs/810-005/102/102.pdf>
- [43] "Solar Rotation Varies by Latitude." [Online]. Available: <https://www.nasa.gov/image-article/solar-rotation-varies-by-latitude/>
- [44] "Esa bulletin," <https://www.esa.int/esapub/bulletin/bullet84/vdbus84.htm>, ESA.
- [45] Dr. R. M. Bonnet - ESA Dr. Wesley T. Huntress - NASA, "SOHO Mission Interruption Joint NASA/ESA," 1998. [Online]. Available: [https://soho.nascom.nasa.gov/operations/Recovery/docs/SOHO\\_final\\_report.html](https://soho.nascom.nasa.gov/operations/Recovery/docs/SOHO_final_report.html)
- [46] "Soho's recovery – an unprecedeted success story," <https://soho.nascom.nasa.gov/operations/Recovery/vandenbu.pdf>, ESA.
- [47] "Leonardo Star Trackers - Flight Experiences and Introduction of SPACESTAR Product on GEO Platforms," [https://indico.esa.int/event/182/contributions/1506/attachments/1456/1682/1710\\_-\\_Boldrini.pdf](https://indico.esa.int/event/182/contributions/1506/attachments/1456/1682/1710_-_Boldrini.pdf), Leonardo Company.
- [48] "Fine pointing sun senso," <https://redwirespace.com/wp-content/uploads/2023/06/redwire-fine-pointing-sun-sensor-flysheet.pdf>, RedWire.

- [49] “Reaction wheel unit,” [https://satsearch.s3.eu-central-1.amazonaws.com/datasheets/satsearch\\_datasheet\\_f04cno\\_bradford\\_reaction-wheel-unit-w18.pdf?X-Amz-Algorithm=AWS4-HMAC-SHA256&X-Amz-Credential=AKIAJLB7IRZ54RAMS36Q%2F20240428%2Feu-central-1%2Fs3%2Faws4\\_request&X-Amz-Date=20240428T160022Z&X-Amz-Expires=86400&X-Amz-Signature=d535a0cafd153275264cc0318a0d5b2dce3ee889592d4393f8ef099298156c44&X-Amz-SignedHeaders=host](https://satsearch.s3.eu-central-1.amazonaws.com/datasheets/satsearch_datasheet_f04cno_bradford_reaction-wheel-unit-w18.pdf?X-Amz-Algorithm=AWS4-HMAC-SHA256&X-Amz-Credential=AKIAJLB7IRZ54RAMS36Q%2F20240428%2Feu-central-1%2Fs3%2Faws4_request&X-Amz-Date=20240428T160022Z&X-Amz-Expires=86400&X-Amz-Signature=d535a0cafd153275264cc0318a0d5b2dce3ee889592d4393f8ef099298156c44&X-Amz-SignedHeaders=host), Bradford Engineering BV.
- [50] “LONG TERM MISSIONS AT THE SUN-EARTH LIBRATION POINT L1: ACE, SOHO, AND WIND,” <https://core.ac.uk/download/pdf/158348809.pdf>, NASA.
- [51] “Soho mission interruption preliminary status and background report - july 15, 1998,” [https://umbra.nascom.nasa.gov/soho/prelim\\_and\\_background\\_rept.html](https://umbra.nascom.nasa.gov/soho/prelim_and_background_rept.html), NASA.
- [52] “LASCO HANDBOOK FOR SCIENTIFIC INVESTIGATORS,” 1994. [Online]. Available: [https://lasco-www.nrl.navy.mil/index.php?p=content/handbook/hndbk\\_7](https://lasco-www.nrl.navy.mil/index.php?p=content/handbook/hndbk_7)
- [53] “SOHO: The Spacecraft,” ESA / NASA. [Online]. Available: <https://soho.nascom.nasa.gov/about/spacecraft.html>
- [54] “Soho mission interruption joint nasa/esa,” [https://soho.nascom.nasa.gov/operations/Recovery/docs/SOHO\\_final\\_report.html](https://soho.nascom.nasa.gov/operations/Recovery/docs/SOHO_final_report.html), NASA.
- [55] “Product Data of Electrodag 501.” [Online]. Available: <https://www.spacematdb.com/spacemat/datasearch.php?name=Electrodag%20501>
- [56] “Product data of PSG 120 FD.” [Online]. Available: <https://www.spacematdb.com/spacemat/datasearch.php?name=PSG%20120%20FD>
- [57] “The application of the thermal control coating PSG120FD. ECSS-Q-70-33A,” ECSS Secretariat, ESA-ESTEC Requirements & Standards Division, Noordwijk, The Netherlands.
- [58] “Product Data of Chemglaze Z306.” [Online]. Available: <https://www.spacematdb.com/spacemat/m-datasearch.php?name=Chemglaze%20Z306>
- [59] Jose L. Garcia, “SOHO SVM Thermal Control,” *SAE Technical Paper Series*, 1994.
- [60] George Dakermanji James C. Leary Richard E. Conde. “The MESSENGER spacecraft”. In: (2006).” [Online]. Available: <https://link.springer.com/content/pdf/10.1007/s11214-007-9269-0.pdf>
- [61] “Soho ancillary data, attitude files.” [Online]. Available: <https://soho.nascom.nasa.gov/gif/sohorotations.gif>
- [62] P. Rumler, H. Schweitzer, H. Evans, “A Performance Evaluation of 2.5 Years in Orbit and Capabilities for a Mission Extension of 5 Years,” *Proceedings of the Fifth European Space Power Conference (ESPC) : Tarragona, Spain, 21-25 September 1998 / organised by European Space Agency [ESA] ... [et al.]. Noordwijk, The Netherlands : ESA Publications Division, 1998. (ESA SP ; 416), p.621*, 1998.
- [63] J. Torsti, E. Valtonen, M. Lumme, P. Peltonen, T. Eronen, M. Louhola, E. Riihonen, G. Schultz, M. Teittinen, K. Ahola, C. Holmlund, V. Kelhä, K. Leppälä, P. Ruuska, and E. Strömmér, “Energetic Particle Experiment ERNE,” *solphys*, vol. 162, no. 1-2, pp. 505–531, 1995.

- [64] Seaton, D. and Berghmans, David and Nicula, B. and Halain, J. and De Groof, Anik and Thibert, Tanguy and Bloomfield, D. and Raftery, Claire and Gallagher, Peter and Auchère, Frédéric and Defise, J. and D'Huys, Elke and Lecat, J. and Mazy, E. and Rochus, P. and Rossi, L. and Schühle, Udo and Slemzin, V. and Yalim, Mehmet Sarp and Zender, Joe, "The swap euv imaging telescope part i: Instrument overview and pre-flight testing," *Solar Physics*, vol. 286, 2012.
- [65] Fiebrich, H., Haines, J., Perol, P., and Rumle, P., "Power system performance of the soho spacecraft during the 1998 attitude recovery," *SAE Technical Paper 1999-01-2484*, 1999.
- [66] "Esa soho science archive." [Online]. Available: <https://ssa.esac.esa.int/ssa/#/pages/search>
- [67] "Space-Qualified Cover Glass," Excelitas Technologies. [Online]. Available: <https://www.excelitas.com/product/space-qualified-cover-glass>
- [68] "SOHO-VIRGO-LOI, Performance Specifications," ESA, 2019. [Online]. Available: <https://sci.esa.int/web/sci-fmi/-/35985-soho-virgo-loi>
- [69] Hovestadt, D., Hilchenbach, M., Bürgi, A., Klecker, B., Laeverenz, P., Scholer, M., "Celia - charge, element and isotope analysis system for soho," *Solar Physics, Volume 162, Issue 1-2, pp. 441-481, 1995*. [Online]. Available: <https://articles.adsabs.harvard.edu//full/1995SoPh..162..441H/0000449.000.html>
- [70] Carl Foley, "CDS SOFTWARE NOTE No. 54," 2003. [Online]. Available: [https://www.mssl.ucl.ac.uk/www\\_solar/soho/cds\\_swnote\\_54.pdf](https://www.mssl.ucl.ac.uk/www_solar/soho/cds_swnote_54.pdf)
- [71] N. Policella, H. Oliveira, and T. Siili, "Managing soho's keyhole periods: Problem definition and solving model," 07 2009.
- [72] "Reaction Wheel Unit W45," Bradford Space. [Online]. Available: <https://satsearch.co/products/bradford-reaction-wheel-unit-w45>